# Chapter 7
# Nonholonomic rolling nonprehensile manipulation primitive

Alejandro Gutierrez-Giles, Aykut C. Satici, Alejandro Donaire, Fabio Ruggiero, Vincenzo Lippiello, Bruno Siciliano

**Abstract** This chapter reviews the problem of nonholonomic rolling in nonprehensile manipulation tasks through two challenging and illustrative examples: the robotic hula-hoop and the ballbot system. The hula-hoop consists of an actuated stick and an unactuated hoop. First, the corresponding kinematic model is derived. Second, the dynamic model is derived through the Lagrange-D'Alembert equations. Then a control strategy is designed to rotate the hoop at some desired constant speed whereas positioning it over a desired point on the stick surface. A stability analysis, which guarantees ultimate boundedness of all signals of interest, is carried out. The ballbot is an underactuated and nonholonomic constrained mobile robot whose upward

Alejandro Gutierrez-Giles
CECAv-UNAM, Av. Universidad 3000, Ciudad Universitaria, CDMX, CP 04510, Mexico, e-mail: alejandro_giles@cecav.unam.mx

Aykut C. Satici
Boise State University, 1910 University Drive, Boise, ID 83709, USA, e-mail: aykutsatici@boisestate.edu

Alejandro Donaire
The University of Newcastle, University Drive, Callaghan, 2308, NSW, Australia, e-mail: alejandro.donaire@newcastle.edu.eu

Fabio Ruggiero
CREATE Consortium & University of Naples Federico II, Department of Electrical Engineering and Information Technology, PRISMA Lab, Via Claudio 21, 80125, Naples, Italy, e-mail: fabio.ruggiero@unina.it

Vincenzo Lippiello
CREATE Consortium & University of Naples Federico II, Department of Electrical Engineering and Information Technology, PRISMA Lab, Via Claudio 21, 80125, Naples, Italy, e-mail: vincenzo.lippiello@unina.it

Bruno Siciliano
CREATE Consortium & University of Naples Federico II, Department of Electrical Engineering and Information Technology, PRISMA Lab, Via Claudio 21, 80125, Naples, Italy, e-mail: bruno.siciliano@unina.it

Table 7.1: Main symbols used in this chapter (pole and hoop are referred to the hula hoop system, ball and top are referred to the ballbot system).

| **Definition** | **Symbol** |
|---|---|
| Frame attached to the pole's and ball's CoM | $\mathcal{H}$ |
| Frame attached to the hoop's and top's CoM | $\mathcal{O}$ |
| Frame attached to the contact point between the hoop and the pole | $\mathcal{C}$ |
| Radius of the pole and the ball | $r_h > 0$ |
| Pole metric tensor | $\mathbf{M}_h \in \mathbb{R}^{2\times 2}$ |
| Pole curvature tensor | $\mathbf{K}_h \in \mathbb{R}^{2\times 2}$ |
| Pole torsion form | $\mathbf{T}_h \in \mathbb{R}^{1\times 2}$ |
| Radius of the hoop | $l_o > 0$ |
| Thickness of the hoop | $2r_o > 0$ |
| Hoop metric tensor | $\mathbf{M}_o \in \mathbb{R}^{2\times 2}$ |
| Hoop curvature tensor | $\mathbf{K}_o \in \mathbb{R}^{2\times 2}$ |
| Hoop torsion form | $\mathbf{T}_o \in \mathbb{R}^{1\times 2}$ |
| Relative curvature tensor | $\tilde{\mathbf{K}}_h \in \mathbb{R}^{2\times 2}$ |
| Relative angular velocities between the contact frames | $\omega_x, \omega_y \; in \mathbb{R}$ |
| Pfaffian matrix | $\mathbf{A}_c \in \mathbb{R}^{3\times 5}$ |
| Generalised coordinates of the pole | $\mathbf{q}_h \in \mathbb{R}^m$ |
| Position of the hoop's centre in $\mathcal{H}$ | $\mathbf{p}_o^h \in \mathbb{R}^3$ |
| Mass of the hoop | $m_o > 0$ |
| Mass of the pole | $m_h > 0$ |
| Gravity acceleration | $g \simeq 9.81$ m/s$^2$ |
| Hoop inertia tensor with respect to $\mathcal{H}$ | $\mathbf{I}_o \in \mathbb{R}^{3\times 3}$ |
| Rotation of $\mathcal{O}$ with respect to $\mathcal{W}$ | $\mathbf{R}_{st} \in SO(3)$ |
| Angular velocity of the hoop in $\mathcal{W}$ | $\boldsymbol{\omega}_o \in \mathbb{R}^3$ |
| Standard unit vectors | $\mathbf{e}_2 = \begin{bmatrix}0 & 1 & 0\end{bmatrix}^T$, $\mathbf{e}_3 = \begin{bmatrix}0 & 0 & 1\end{bmatrix}^T$ |
| Distance from the ball's CoM and the top's CoM | $l > 0$ |
| Position of the ball with respect to $\mathcal{W}$ | $\mathbf{p}_{sb} \in \mathbb{R}^3$ |
| Angular velocity of the ball with respect to $\mathcal{W}$ | $\boldsymbol{\omega}_{sb} \in \mathbb{R}^3$ |
| Rotation of $\mathcal{H}$ with respect to $\mathcal{W}$ | $\mathbf{R}_{sb} \in SO(3)$ |
| Angular velocity of the top with respect to $\mathcal{W}$ | $\boldsymbol{\omega}_{st} \in \mathbb{R}^3$ |
| Linear velocity of the top with respect to $\mathcal{W}$ | $\mathbf{v}_{st} \in \mathbb{R}^3$ |
| Linear velocity of the ball with respect to $\mathcal{W}$ | $\mathbf{v}_{sb} \in \mathbb{R}^3$ |
| Angular velocity of the top with respect to the ball | $\boldsymbol{\omega}_{bt} \in \mathbb{R}^3$ |
| Position of the top with respect to $\mathcal{W}$ | $\mathbf{p}_{st} \in \mathbb{R}^3$ |
| Inertia tensor of the ball with respect to $\mathcal{W}$ | $\mathbf{I}_b \in \mathbb{R}^{3\times 3}$ |
| Inertia tensor of the top with respect to $\mathcal{W}$ | $\mathbf{I}_t \in \mathbb{R}^{3\times 3}$ |
| Mass of the ball | $m_b > 0$ |
| Mass of the top | $m_t > 0$ |

equilibrium point must be stabilised by active controls. Coordinate-invariant equations of motion are derived for the ballbot. The linearised equations of motion are then derived, followed by the detailed controllability analysis. Excluding the rotary degree of freedom of the ball in the inertial vertical direction, the linear system turns out to be controllable. It follows that the nonlinear system is locally controllable, and a proportional-derivative type

controller is designed to locally exponentially stabilise the upward equilibrium point and the translation of the ball. Numerical simulations for these two examples illustrate the effectiveness of the proposed methods.
This chapter is based on the works presented in [117, 118, 268, 270].

## 7.1 Brief introduction

In the previous chapter, the manipulation problem of nonprehensile planar rolling systems has been addressed. In planar rolling systems, the kinematic constraint associated with the pure rolling motion (only rolling, no sliding) is integrable. Therefore, the system is holonomic. In this chapter, the focus is shifted towards 3D systems in which the pure rolling constraint is not integrable. A system with a set of kinematic constraints, expressed in the so-called Pfaffian form [284], in which at least one of these constraints is not integrable is said to be a nonholonomic system. A nonholonomic constraint implies that some motion directions are instantaneously not allowed.

Therefore, this chapter tackles controlling an object manipulated through nonholonomic rolling motions without form or force closure grasps. The ball-on-plate gives the most illustrative example of it [276]. The primary objective is to steer the free-rolling sphere toward the desired position and/or orientation or along a desired path. It is worth pointing out that most of the works addressing the ball-and-plate application consider the prehensile case obtained by caging the sphere between two plates [74, 190, 234]. In such a configuration, one plate is actuated while the other one is fixed. Dismissing the fixed plate, the ball-and-plate application is addressed as a nonprehensile rolling manipulation system in which the sole supporting moving plate controls the ball. Therefore, position control of a basketball on a plate is tackled in [166]. An analysis of the kinematics of rolling, based on a coordinate-free approach, considering the cases of either pure rolling or twist-rolling, is proposed in [71]. An extension of the DoD to the 3D case is given by the stabilization of a ball free to roll on an actuated sphere in full gravity [103, 177].

This chapter first presents a control design for the hula-hoop task, which belongs to the nonholonomic rolling nonprehensile manipulation primitive. From a robotic point of view, this can be schematized through a hoop freely rolling around an actuated pole. A first mathematical derivation was proposed in [227] without taking correctly into account the nonholonomic constraints. This issue is overcome in [117], in which a control approach without velocity measurement is proposed. A formal mathematical analysis that guarantees ultimate boundedness of all coordinates is developed in [118].

Afterwards, this chapter addresses the control design for the ballbot. The ballbot is an underactuated, nonholonomically constrained, mobile robot whose upward equilibrium point has to be stabilised by active controls [270, 268]. The ballbot is thus a spherical robot with a turret that is actively con-

trolled on a plane. It is very similar to the ball-on-plate problem but, in this case, the actuation is in the sphere and not in the plate.

The outline of the chapter shows then the two examples depicted above with modelling, control design, and simulation results.

## 7.2 The hula-hoop problem

The task consists of spinning the hoop around a stick at some desired angular speed while simultaneously driving the hoop to an arbitrarily desired point over the pole surface. First, the kinematic model is derived. Second, the dynamic model is derived through the Lagrange–D'Alembert equations. Then a control strategy is designed to rotate the hoop at some desired constant speed whereas positioning it over a desired point on the stick surface. A stability analysis, which guarantees ultimate boundedness of all signals of interest, is carried out. Finally, numerical simulations illustrate the effectiveness of the proposed method.

### 7.2.1 Contact kinematics

A draw of the hoop and pole system considered in this work is shown in Figure 7.1, where the inertial, pole (hand), hoop (object), and contact Cartesian frames are displayed, which in the subsequent are denoted by $\mathcal{W}$, $\mathcal{H}$, $\mathcal{O}$, and $\mathcal{C}$, respectively. A given coordinate frame $\mathcal{X}$ consists of an origin vector $\mathbf{o}_x \in \mathbb{R}^3$, and three orthonormal unit vectors $\mathbf{x}_x, \mathbf{y}_x, \mathbf{z}_x \in \mathbb{R}^3$. The contact frame $\mathcal{C}$ is defined as follows: $\mathbf{o}_c$ is located at the contact point, $\mathbf{x}_c$ is in the line connecting the hoop centre with the contact point and pointing outwards the pole, $\mathbf{z}_c$ is normal to the hoop equatorial plane passing through $\mathbf{o}_c$, and $\mathbf{y}_c$ is chosen to form an orthonormal frame.

In this section, the following notation is adopted: $\mathbf{v}_i^j$ means that the vector $\mathbf{v}_i$ is referenced to the $j$ frame. When a vector or matrix is referenced to the world coordinate frame the superscript $(\cdot)^w$ is obviated.

The next coordinates are defined to describe the pole surface:

- $\theta \in \mathbb{R}$: an angle from one arbitrarily defined point on the pole surface to the contact point, measured by taking $\mathbf{z}_h$ as the rotation axis.
- $z_o > 0$: a distance form the origin $\mathbf{o}_h$ to the contact point over the $\mathbf{z}_h$ axis.

Defining the vector $\boldsymbol{\alpha}_h = \begin{bmatrix}\theta & z_0\end{bmatrix}^T \in \mathbb{R}^2$, the pole surface in local coordinates is described by

$$\mathbf{c}_h(\boldsymbol{\alpha}_h) = \begin{bmatrix} r_h c_\theta & r_h s_\theta & z_o \end{bmatrix}^T \in \mathbb{R}^3 \,, \tag{7.1}$$

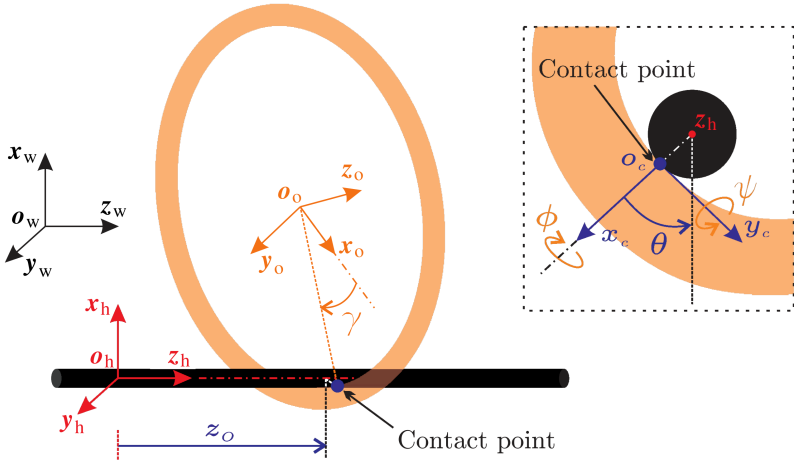


Fig. 7.1: Sketch of the pole and hoop system.

where $c_\theta = \cos(\theta)$ and $s_\theta = \sin(\theta)$ . The tangent vectors are computed as

$$\mathbf{c}_{h_u} = \begin{bmatrix} -r_h s_\theta & r_h c_\theta & 0 \end{bmatrix}^T \in \mathbb{R}^3 \tag{7.2}$$

$$\mathbf{c}_{h_v} = \begin{bmatrix} 0 & 0 & 1 \end{bmatrix}^T \in \mathbb{R}^3 . \tag{7.3}$$

It can be easily verified that $\|\mathbf{c}_{h_u}\| = r_h$ and $\|\mathbf{c}_{h_v}\| = 1$. The corresponding normal vector is given by

$$\mathbf{n}_h = \begin{bmatrix} c_\theta & s_\theta & 0 \end{bmatrix}^T \in \mathbb{R}^3 , \tag{7.4}$$

with partial derivatives

$$\mathbf{n}_{h_u} = \begin{bmatrix} -s_\theta & c_\theta & 0 \end{bmatrix}^T \in \mathbb{R}^3 \tag{7.5}$$

$$\mathbf{n}_{h_v} = \mathbf{0_3}. \tag{7.6}$$

The second-order partial derivatives of $\mathbf{c}_{h_u}$, necessary to compute the torsion, are

$$\mathbf{c}_{h_{uu}} = \begin{bmatrix} -r_h c_\theta & -r_h s_\theta & 0 \end{bmatrix}^T \in \mathbb{R}^3 \tag{7.7}$$

$$\mathbf{c}_{h_{uv}} = \mathbf{0_3}. \tag{7.8}$$

Therefore, following the definitions given in [207], the metric and curvature tensors and the torsion form of the pole surface are

$$\mathbf{M}_h = \begin{bmatrix} r_h & 0 \\ 0 & 1 \end{bmatrix} , \quad \mathbf{K}_h = \begin{bmatrix} 1/r_h & 0 \\ 0 & 0 \end{bmatrix} , \quad \mathbf{T}_h = \begin{bmatrix} 0 & 0 \end{bmatrix} .$$

On the other hand, the following local coordinates for describing the hoop surface are defined:

- $\gamma \in \mathbb{R}$: an angle from one arbitrarily defined point in the hoop surface to the contact point measured by taking $\mathbf{z}_o$ as the rotation axis.
- $\psi \in \mathbb{R}$: an angle of the equatorial plane of the hoop over $\mathbf{y}_c$.

Collect $\boldsymbol{\alpha}_o = \begin{bmatrix}\gamma & \psi\end{bmatrix}^T \in \mathbb{R}^2$ such that the hoop surface in local coordinates is described by

$$\mathbf{c}_o(\boldsymbol{\alpha}_o) = \begin{bmatrix}-(l_o - r_o c_\psi)c_\gamma & (l_o - r_o c_\psi)s_\gamma & -r_o s_\psi\end{bmatrix}^T \in \mathbb{R}^3. \tag{7.9}$$

Therefore, the corresponding tangent vectors are computed as

$$\mathbf{c}_{o_u} = \begin{bmatrix}-(l_o - r_o c_\psi)s_\gamma & (l_o - r_o c_\psi)c_\gamma & 0\end{bmatrix}^T \in \mathbb{R}^3 \tag{7.10}$$

$$\mathbf{c}_{f_v} = \begin{bmatrix}r_o c_\gamma s_\psi & r_o s_\gamma s_\psi & -r_o c_\psi\end{bmatrix}^T \in \mathbb{R}^3\,. \tag{7.11}$$

In such case, $\|\mathbf{c}_{o_u}\| = l_o - r_o c_\psi$ and $\|\mathbf{c}_{o_v}\| = r_o$. The normal vector is given by

$$\mathbf{n}_o = \begin{bmatrix}-c_\gamma c_\psi & -s_\gamma c_\psi & -s_\psi\end{bmatrix}^T \in \mathbb{R}^3\,, \tag{7.12}$$

with partial derivatives

$$\mathbf{n}_{o_u} = \begin{bmatrix}s_\gamma c_\psi & -c_\gamma c_\psi & 0\end{bmatrix}^T \in \mathbb{R}^3 \tag{7.13}$$

$$\mathbf{n}_{o_v} = \begin{bmatrix}c_\gamma s_\psi & s_\gamma s_\psi & -c_\psi\end{bmatrix}^T \in \mathbb{R}^3\,. \tag{7.14}$$

The second order partial derivatives of $\mathbf{c}_{o_u}$ are

$$\mathbf{c}_{o_{uu}} = \begin{bmatrix}-(l_o - r_o c_\psi)c_\gamma & -(l_o - r_o c_\psi)s_\gamma & 0\end{bmatrix}^T \in \mathbb{R}^3 \tag{7.15}$$

$$\mathbf{c}_{o_{uv}} = \begin{bmatrix}-r_o s_\gamma s_\psi & r_o c_\gamma s_\psi & 0\end{bmatrix}^T \in \mathbb{R}^3\,. \tag{7.16}$$

Regarding the hoop's surface, the metric and curvature tensors and the torsion form are given by

$$\mathbf{M}_o = \begin{bmatrix}l_o - r_o c_\psi & 0\\ 0 & r_o\end{bmatrix}, \quad \mathbf{K}_o = \begin{bmatrix}-c_\psi/(l_o - r_o c_\psi) & 0\\ 0 & 1/r_o\end{bmatrix},$$
$$\mathbf{T}_o = \begin{bmatrix}-s_\psi/(l_o - r_o c_\psi) & 0\end{bmatrix}.$$

An additional coordinate, necessary to compute the contact kinematics, $\phi \in \mathbb{R}$ is the angle form $\mathbf{c}_{hu}$ to $\mathbf{c}_{ou}$, measured over the $\mathbf{x}_c$ axis. Thus, the relative curvature is computed to be

$$\widetilde{\mathbf{K}}_h = \frac{1}{r_h}\begin{bmatrix}c_\phi^2 & -s_\phi c_\phi\\ -s_\phi c_\phi & s_\phi^2\end{bmatrix}. \tag{7.17}$$

Now, by combining both surface geometric parameters, the Montana's equations in terms of the relative velocities between the contact frames, assuming a pure rolling, are given by

$$\begin{bmatrix}\dot{\gamma}\\ \dot{\psi}\end{bmatrix} = \frac{1}{l_o c_\phi^2 - (r_h + r_o)c_\psi}\begin{bmatrix} r_h + r_o s_\phi^2 & r_o s_\phi c_\phi \\ (l_o - r_o c_\psi)s_\phi c_\phi & (l_o - r_o c_\psi)c_\phi^2 - r_h c_\psi\end{bmatrix}\begin{bmatrix}-\omega_y\\ \omega_x\end{bmatrix} \tag{7.18}$$

$$\begin{bmatrix}\dot{\theta}\\ \dot{z}_o\end{bmatrix} = \frac{1}{l_o c_\phi^2 - (r_h + r_o)c_\psi}\begin{bmatrix} (l_o - r_o c_\psi)c_\phi & r_o s_\phi c_\psi \\ -(l_o - r_o c_\psi)(r_h + r_o)s_\phi & -r_o c_\phi\,(l_o - (r_h + r_o)c_\psi)\end{bmatrix}\begin{bmatrix}-\omega_y\\ \omega_x\end{bmatrix} \tag{7.19}$$

$$\dot{\phi} = \frac{(r_h + r_o s_\phi^2)s_\psi\omega_y - r_o s_\phi c_\phi s_\psi \omega_x}{l_o c_\phi^2 - (r_h + r_o)c_\psi}\,. \tag{7.20}$$

Let the contact coordinates vector be defined by

$$\mathbf{q}_c = \begin{bmatrix}\gamma & \psi & \theta & z_o & \phi\end{bmatrix}^T \in \mathbb{R}^5. \tag{7.21}$$

Thus, the kinematic equations (7.18)–(7.20) can be rewritten as

$$\dot{\mathbf{q}}_c = \mathbf{g}_1\omega_x + \mathbf{g}_2\omega_y\,, \tag{7.22}$$

where

$$\mathbf{g}_1 = \frac{1}{l_o c_\phi^2 - (r_o + r_o)c_\psi}\begin{bmatrix} r_o s_\phi c_\phi \\ (l_o - r_o c_\psi)c_\phi^2 - r_o c_\psi \\ r_o s_\phi c_\psi \\ -r_o c_\phi\,(l_o - (r_o + r_o)c_\psi) \\ -r_o s_\phi c_\phi s_\psi\end{bmatrix} \in \mathbb{R}^5 \tag{7.23}$$

$$\mathbf{g}_2 = \frac{1}{l_o c_\phi^2 - (r_o + r_o)c_\psi}\begin{bmatrix} -(r_o + r_o s_\phi^2) \\ -(l_o - r_o c_\psi)s_\phi c_\phi \\ -(l_o - r_o c_\psi)c_\phi \\ (l_o - r_o c_\psi)(r_o + r_o)s_\phi \\ (r_o + r_o s_\phi^2)s_\psi\end{bmatrix} \in \mathbb{R}^5. \tag{7.24}$$

Assume that the hoop thickness can be neglected, *i.e.,* $r_o = 0$. Therefore, by choosing a basis for the left null space of $\mathbf{G} = \begin{bmatrix}\mathbf{g}_1 & \mathbf{g}_2\end{bmatrix}$, a set of Pffafian constraints [216, p. 320] can be constructed as follows

$$\mathbf{A}_c(\mathbf{q}_c)\dot{\mathbf{q}}_c = \mathbf{0}_3\,, \tag{7.25}$$

where

$$\mathbf{A}_c(\mathbf{q}_c) = \begin{bmatrix} -l_o c_\phi/r_o & 0 & 1 & 0 & 0 \\ s_\psi & 0 & 0 & 1 & 0 \\ l_o s_\phi & 0 & 0 & 0 & 1\end{bmatrix}\,. \tag{7.26}$$

At this point, an arbitrary number of degrees of freedom for the pole is considered. The generalised coordinates of the pole express its pose (position and orientation) in the Cartesian space. As one of the goals of this work is to have the best controllability properties with the least actuated coordinates, the configuration space for the pole will be chosen after the controllability analysis given later in this section. Now, define the vectors $\mathbf{q}_r = \begin{bmatrix}\gamma & \psi & \mathbf{q}_h\end{bmatrix}^T \in \mathbb{R}^{m+2}$, $\mathbf{q}_s = \begin{bmatrix}\theta & \phi & z_o\end{bmatrix}^T \in \mathbb{R}^3$, and $\mathbf{q} = \begin{bmatrix}\mathbf{q}_r & \mathbf{q}_s\end{bmatrix}^T \in \mathbb{R}^{m+5}$. Then, the constraints (7.26) can be written as

$$\mathbf{A}_r(\mathbf{q})\dot{\mathbf{q}}_r + \dot{\mathbf{q}}_s = \mathbf{0}\,, \tag{7.27}$$

where

$$\mathbf{A}_r(\mathbf{q}) = \begin{bmatrix} -l_o c_\phi / r_o & 0 & 0 & \cdots & 0 \\ s_\psi & 0 & 0 & \cdots & 0 \\ l_o s_\phi & 0 & 0 & \cdots & 0 \end{bmatrix}. \tag{7.28}$$

### 7.2.2 Dynamic model

The vector $\mathbf{p}_o^h$ can be expressed in terms of the generalised coordinates is expressed as follows

$$\mathbf{p}_o^h = \begin{bmatrix} -l_o c_\theta c_\psi + r_o c_\theta + l_o s_\theta s_\phi s_\psi \\ r_o s_\theta - l_o c_\psi s_\theta - l_o c_\theta s_\phi s_\psi \\ l_o s_\psi + z_o \end{bmatrix}. \tag{7.29}$$

Given the expressions $\mathbf{I}_o = \operatorname{diag}\left\{\frac{1}{2}m_o l_o^2, \frac{1}{2}m_o l_o^2, m_o l_o^2\right\}$ and

$$\mathbf{R}_o = \begin{bmatrix} c_\psi c_\theta - s_\phi s_\psi s_\theta & -c_\phi s_\theta & c_\theta s_\psi + c_\psi s_\phi s_\theta \\ c_\theta s_\phi s_\psi + c_\psi s_\theta & c_\phi c_\theta & -c_\psi c_\theta s_\phi + s_\psi s_\theta \\ -c_\phi s_\psi & s_\phi & c_\phi c_\psi \end{bmatrix}, \tag{7.30}$$

the hoop angular velocity can be obtained from $\mathbf{R}_{st}$ through $\mathbf{S}(\boldsymbol{\omega}_o) = \dot{\mathbf{R}}_o \mathbf{R}_o^T$, where $\mathbf{S}(\boldsymbol{\omega}_o)$ is a well–known skew symmetric matrix constructed from $\boldsymbol{\omega}_o$. The angular velocity can be computed from

$$\boldsymbol{\omega}_o = \begin{bmatrix} c_\theta \dot{\phi} - c_\phi s_\theta \dot{\psi} \\ s_\theta \dot{\phi} + c_\phi c_\theta \dot{\psi} \\ s_\phi \dot{\psi} + \dot{\theta} \end{bmatrix}. \tag{7.31}$$

The Lagrange–d'Alembert equations, subject to the Pfaffian constraints above, are given by

$$\left(\frac{\mathrm{d}}{\mathrm{d}t}\frac{\partial \mathcal{L}}{\partial \dot{\mathbf{q}}_r} - \frac{\partial \mathcal{L}}{\partial \mathbf{q}_r} - \boldsymbol{\Upsilon}_r\right) - \mathbf{A}_r^T(\mathbf{q})\left(\frac{\mathrm{d}}{\mathrm{d}t}\frac{\partial \mathcal{L}}{\partial \dot{\mathbf{q}}_s} - \frac{\partial \mathcal{L}}{\partial \mathbf{q}_s}\right) = \mathbf{0}_{\mathbf{m+2}}\,, \tag{7.32}$$

where

$$\boldsymbol{\Upsilon}_r = \begin{bmatrix} \mathbf{0}_2 \\ \mathbf{u} \end{bmatrix}, \tag{7.33}$$

with $\mathbf{u} \in \mathbb{R}^m$ the vector of generalised forces acting on the pole and $\mathcal{L} \in \mathbb{R}$ the system Lagrangian available in [117].

The vectors $\dot{\mathbf{q}}_s$ and $\ddot{\mathbf{q}}_s$ can be eliminated by following the procedure described in [216, Ch. 6], which results in the following dynamic model

$$\mathbf{B}_o(\mathbf{q})\ddot{\mathbf{q}}_o + \mathbf{c}_o(\mathbf{q}, \dot{\mathbf{q}}_o) + \mathbf{T}_o(\mathbf{q})\ddot{\mathbf{q}}_h = \mathbf{0}, \tag{7.34a}$$

$$\mathbf{B}_h(\mathbf{q})\ddot{\mathbf{q}}_h + \mathbf{c}_h(\mathbf{q}, \dot{\mathbf{q}}_o) + \mathbf{T}_o^T(\mathbf{q})\ddot{\mathbf{q}}_o = \mathbf{u}\,, \tag{7.34b}$$

where $\mathbf{q}_o = \begin{bmatrix} \gamma & \psi \end{bmatrix}^T \in \mathbb{R}^2$, $\mathbf{B}_o(\mathbf{q}) \in \mathbb{R}^{2\times 2}$ is the inertia matrix of the hoop, $\mathbf{B}_h(\mathbf{q}) \in \mathbb{R}^{m\times m}$ is the inertia matrix of the pole, $\mathbf{c}_o(\mathbf{q}, \dot{\mathbf{q}}_o) \in \mathbb{R}^2$ is the Coriolis term related to hoop, $\mathbf{c}_h(\mathbf{q}, \dot{\mathbf{q}}_o) \in \mathbb{R}^m$ is the Coriols term related to the pole, and $\mathbf{T}_o(\mathbf{q}) \in \mathbb{R}^{2\times m}$ is the inertia coupling matrix whose effects are analysed below. Notice that $\mathbf{B}_o(\mathbf{q})$ is always invertible. Thus, equation (7.34b) can be solved for $\ddot{\mathbf{q}}_h$ and substituted into (7.34a) to obtain

$$\mathbf{M}_r(\mathbf{q})\ddot{\mathbf{q}}_o + \mathbf{c}_r(\mathbf{q}, \dot{\mathbf{q}}_o) = \mathbf{T}_r(\mathbf{q})\mathbf{u}\,, \tag{7.35}$$

where

$$\mathbf{M}_r(\mathbf{q}) = \mathbf{B}_o(\mathbf{q}) - \mathbf{T}_o(\mathbf{q})\mathbf{B}_h^{-1}(\mathbf{q})\mathbf{T}_o^T(\mathbf{q}) \tag{7.36}$$

$$\mathbf{c}_r(\mathbf{q}, \dot{\mathbf{q}}_o) = \mathbf{c}_o(\mathbf{q}, \dot{\mathbf{q}}_o) - \mathbf{T}_o(\mathbf{q})\mathbf{B}_h^{-1}(\mathbf{q})\mathbf{c}_h(\mathbf{q}, \dot{\mathbf{q}}_o) \tag{7.37}$$

$$\mathbf{T}_r(\mathbf{q}) = -\mathbf{T}_o(\mathbf{q})\mathbf{B}_h^{-1}(\mathbf{q})\,. \tag{7.38}$$

The dynamic model (7.35) can be further simplified to obtain

$$\ddot{\mathbf{q}}_o = \mathbf{f}(\mathbf{q}, \dot{\mathbf{q}}_o) + \mathbf{g}(\mathbf{q})\mathbf{u}\,, \tag{7.39}$$

with the definitions $\mathbf{f}(\mathbf{q}, \dot{\mathbf{q}}_o) = -\mathbf{M}_r^{-1}(\mathbf{q})\mathbf{c}_r(\mathbf{q}, \dot{\mathbf{q}}_o)$, and $\mathbf{g}(\mathbf{q}) = \mathbf{M}_r^{-1}(\mathbf{q})\mathbf{T}_r(\mathbf{q})$. The model (7.34) represents the dynamics of the hula-hoop system along with the nonholonomic constraints (7.27), which are equivalent to

$$\dot{\theta} = \frac{l_o c_\phi}{r_h}\dot{\gamma} \tag{7.40}$$

$$\dot{z}_o = -l_o s_\phi \dot{\gamma} \tag{7.41}$$

$$\dot{\phi} = -s_\psi \dot{\gamma}\,. \tag{7.42}$$

The inertial coupling matrix plays a crucial role for underactuated mechanical systems. In the present case, if $rank(\mathbf{T}_o(\mathbf{q})) = 2, \forall \mathbf{q}$, the underactuated system is said to be *strong inertially coupled* [296]. Whenever the mechanical system is strong inertially coupled, the Penrose's right pseudo-inverse matrix

$$\mathbf{T}_o^+ = \mathbf{T}_o^T \left( \mathbf{T}_o \mathbf{T}_o^T \right)^{-1} \tag{7.43}$$

is well defined and the following orthogonal projection matrices can be constructed

$$\mathbf{P}_o = \mathbf{T}_o^+ \mathbf{T}_o \in \mathbb{R}^{m \times m} \tag{7.44}$$

$$\mathbf{Q}_o = \mathbf{I}_m - \mathbf{P}_o \in \mathbb{R}^{m \times m} . \tag{7.45}$$

Notice that $\mathbf{P}_o$ projects every $\mathbb{R}^m$-vector onto the rank space of $\mathbf{T}_o$. Conversely, $\mathbf{Q}_o$ makes the projection into the null space of $\mathbf{T}_o$. It is straightforward to verify that the following relations hold: $\mathbf{P}_o \mathbf{T}_o^T = \mathbf{T}_o^T$, $\mathbf{T}_o \mathbf{P}_o = \mathbf{T}_o$, $\mathbf{Q}_o \mathbf{T}_o^T = \mathbf{O}_{2 \times m}$, and $\mathbf{T}_o \mathbf{Q}_o = \mathbf{O}_2$.

#### 7.2.2.1 Controllability analysis

The controllability of the system (7.34a)–(7.34b) depends on the configuration of the pole. Several configurations of interest, namely (*i*) two rotations ($m = 2$), (*ii*) three translations ($m = 3$), (*iii*) two rotations plus two translations ($m = 4$), and (*iv*) three rotations plus three translations ($m = 6$), have been analysed in this work with the aid of a symbolic computing software (*Wolfram Mathematica* [1]). The corresponding dynamic model is strong inertially coupled for all the configurations mentioned above. Therefore, the main motivation for the comparison is to find the configuration with fewer degrees of freedom having the best controllability properties. The conclusions below are valid for all the cases mentioned.

For the model (7.34a)–(7.34b) the gravity torque of the underactuated part is not constant. The inertia matrix depends on the unactuated variables, so it never satisfies the structural necessary and sufficient conditions given in [233], and the nonholonomic constraints are of the *second-order* kind. As a consequence, the dynamic system is *strongly accessible* [258]. That means that, in principle, every possible configuration can be reached. However, this strong accessibility property "is far from being sufficient for the existence of a feedback control which asymptotically stabilises the underactuated system" [258]. For the system (7.34a)–(7.34b), it turns out from [40] that the Brockett's necessary condition for the existence of a continuous asymptotically stabilizing feedback control law is equivalent to check if the image of

$$\mathbf{B}_o^{-1}(\mathbf{q}) \mathbf{c}_o(\mathbf{q}, \dot{\mathbf{q}}_r) \tag{7.46}$$

contains a neighbourhood of the origin in $\mathbb{R}^2$. This condition is satisfied by all the case studies, although it does not imply that there exists such a control law.

[1] `https://www.wolfram.com`

The so-called *small time local controllability* (STLC) is a stronger notion of controllability, which guarantees the existence of a piece-wise asymptotic stabilizing feedback control law [304]. The STLC property also guarantees the existence of an asymptotic stabilizing continuous time-periodic controller [64]. A sufficient condition to check the STLC property for mechanical systems is given in [258]. Unfortunately, this condition is not met by any of the case studies, and thus no conclusion can be made about the STLC property for the system (7.34a)–(7.34b). A necessary and sufficient condition for the STLC is given in [305]. Regrettably, this condition is much more challenging to check, even with the help of symbolic computing software.

Finally, the controller design and the dynamic analysis can be simplified by transforming the system into a *normal form* as proposed in [232]. Once again, this sufficient condition is not met by any of the cases under consideration.

### 7.2.3 Controller design and stability analysis

The control objective is to spin the hoop at a desired angular velocity $\dot{\gamma}_d > 0$, while simultaneously driving it to the desired position $z_{od} \in \mathbb{R}$ over the pole surface, and maintaining it perpendicular to the pole. A design of a feedback model-based control for (7.34a)–(7.42) is a challenging problem from the control point of view. Some of the main difficulties are listed below.

- The kinematic constraints (7.40)–(7.42) are completely nonholonomic [216, p. 320]. In addition, the relative grow vector of the related control system is $(2, 1, 2)$, and then it cannot be transformed into a chained form [76, p. 319].
- The model (7.34a)–(7.34b) is underactuated, and in the simplest case the shape coordinates are not actuated. Therefore, the result of [82] cannot be applied. In the remaining cases, the inertia matrices depend on both actuated and unactuated coordinates.
- The system trajectories must satisfy the nonholonomic constraints (7.40)–(7.42), hence it is not clear whether it is possible to induce a periodic motion for the unactuated coordinates satisfying the control objective stated above, which is a crucial step to apply the methodology of [281, 282].
- Because of the nonholonomic nature of the system, the control objective cannot be translated into a regulation problem, but it must be ensured tracking on the unactuated coordinates, for which the result of [81] does not apply.

Given the difficulties for designing a standard controller for the system under study, in the following development an *ad-hoc* strategy is employed to satisfy the control objective.

Let the input $\mathbf{u}$ be defined as

$$\mathbf{u} = \mathbf{B}_h \left( \mathbf{P}_o \mathbf{u}_P + \mathbf{Q}_o \mathbf{u}_Q \right) , \tag{7.47}$$

where $\mathbf{u}_P \in \mathbb{R}^m$ and $\mathbf{u}_Q \in \mathbb{R}^m$ are two independent inputs belonging to orthogonal subspaces. Taking into account (7.35), the noncollocated partial feedback linearisation (NPFL) [296] input can be defined as

$$\mathbf{u}_P = -\mathbf{T}_o^+ \left( \mathbf{c}_r + \mathbf{M}_r \mathbf{v}_P \right) , \tag{7.48}$$

with $\mathbf{v}_P \in \mathbb{R}^2$ a virtual control input to design. Because $\mathbf{M}_r$ is always full rank [115], it can be obtained

$$\ddot{\mathbf{q}}_o = \mathbf{v}_P \, , \tag{7.49}$$

with zero dynamics given in (7.70).

The control objective for the hoop coordinates consists in designing the input $\mathbf{v}_P$ to drive $\dot{\gamma} \to \dot{\gamma}_d$ and $(z_o, \psi, \phi) \to (z_{od}, 0, 0)$, while satisfying the nonholonomic constraints (7.40)–(7.42). For this purpose, first define

$$\boldsymbol{\xi} = \begin{bmatrix} \xi_1 \\ \xi_2 \\ \xi_3 \end{bmatrix} = \begin{bmatrix} z_o - z_{od} \\ -l_o s_\phi \\ l_o c_\phi s_\psi \end{bmatrix} \in \mathbb{R}^3, \tag{7.50}$$

whose time derivative are

$$\dot{\boldsymbol{\xi}} = \begin{bmatrix} \dot{\xi}_1 \\ \dot{\xi}_2 \\ \dot{\xi}_3 \end{bmatrix} = \begin{bmatrix} \xi_2 \dot{\gamma} \\ \xi_3 \dot{\gamma} \\ l_o s_\phi s_\psi^2 \dot{\gamma} + l_o c_\phi c_\psi \dot{\psi} \end{bmatrix} . \tag{7.51}$$

Next, consider the auxiliary definitions

$$\boldsymbol{\eta} = \begin{bmatrix} \eta_1 \\ \eta_2 \end{bmatrix} = \begin{bmatrix} \dot{\gamma} - \dot{\gamma}_d \\ \dot{\psi} - f_\psi \end{bmatrix} \in \mathbb{R}^2, \tag{7.52}$$

where

$$f_\psi = f_\psi(\psi, \phi, \dot{\gamma}, \boldsymbol{\xi}) = -\left( l_o s_\phi s_\psi^2 + \mathbf{k}_\xi^T \boldsymbol{\xi} \right) \frac{\dot{\gamma}}{l_o c_\phi c_\psi} \, , \tag{7.53}$$

defined for $-\pi/2 < \phi, \psi < \pi/2$, with $\mathbf{k}_\xi = \begin{bmatrix} k_{\xi 1} & k_{\xi 2} & k_{\xi 3} \end{bmatrix}^T \in \mathbb{R}^3$ a vector of positive constant gains. Substituting (7.52) into (7.51) yields

$$\dot{\boldsymbol{\xi}} = \begin{bmatrix} \xi_2 \dot{\gamma}_d + \xi_2 \eta_1 \\ \xi_3 \dot{\gamma}_d + \xi_3 \eta_1 \\ -\mathbf{k}_\xi^T \boldsymbol{\xi} \dot{\gamma}_d - \mathbf{k}_\xi^T \boldsymbol{\xi} \eta_1 + l_o c_\phi c_\psi \eta_2 \end{bmatrix} . \tag{7.54}$$

In order to carry out the dynamic analysis, define the state

$$\boldsymbol{\zeta} = \begin{bmatrix} \boldsymbol{\xi}^T & \boldsymbol{\eta}^T \end{bmatrix}^T \in \mathbb{R}^5. \tag{7.55}$$

*Proposition 7.2.1* [118] Define the region $B_r = \{\boldsymbol{\zeta} : \|\boldsymbol{\zeta}\| \leq l_o\}$ and let the control law be given by

$$\mathbf{v}_P = \begin{bmatrix} v_{P1} \\ v_{P2} \end{bmatrix} = \begin{bmatrix} -k_{\eta 1}\eta_1 \\ \dfrac{\mathrm{d}}{\mathrm{d}t} f_\psi - k_{\eta 2}\eta_2 \end{bmatrix}, \tag{7.56}$$

where $k_{\eta 1}, k_{\eta 2} > 0$. There exists a bounded region $B_\delta \subset B_r$, and a combination of gains $\mathbf{k}_\xi, k_{\eta 1}, k_{\eta_2}$ in (7.53) and (7.56), such that if the initial condition satisfies $\boldsymbol{\zeta}(t_0) \in B_\delta$, then $\boldsymbol{\zeta}(t) \in B_r\,, \forall t \geq t_0$. Furthermore, the system trajectories are ultimately bounded within an arbitrarily small region $B_\mu \subset B_r$, centred at the origin. □

*Proof* If $\boldsymbol{\eta} = \mathbf{0}_2$ in (7.54) one gets

$$\dot{\boldsymbol{\xi}} = \begin{bmatrix} 0 & 1 & 0 \\ 0 & 0 & 1 \\ -k_{\xi 1} & -k_{\xi 2} & -k_{\xi 3} \end{bmatrix} \boldsymbol{\xi} = \mathbf{A}_\xi \boldsymbol{\xi}\,, \tag{7.57}$$

that is a linear time-invariant system with $\mathbf{A}_\xi \in \mathbb{R}^{3\times 3}$ a Hurwitz matrix. A well-established result of linear control [152, Theorem 4.6] states that there exist two symmetric positive definite matrices $\mathbf{P}_\xi \in \mathbb{R}^{3\times 3}$ and $\mathbf{Q}_\xi \in \mathbb{R}^{3\times 3}$ satisfying

$$\mathbf{A}_\xi^T \mathbf{P}_\xi + \mathbf{P}_\xi \mathbf{A}_\xi = -\mathbf{Q}_\xi\,. \tag{7.58}$$

These matrices satisfy the bounds $\lambda_{Pm}\|\mathbf{x}\|^2 \leq \mathbf{x}^T\mathbf{P}_\xi\mathbf{x} \leq \lambda_{PM}\|\mathbf{x}\|^2$ and $\lambda_{Qm}\|\mathbf{x}\|^2 \leq \mathbf{x}^T\mathbf{Q}_\xi\mathbf{x} \leq \lambda_{QM}\|\mathbf{x}\|^2$ for every vector $\mathbf{x} \in \mathbb{R}^3$, with $0 < \lambda_{Pm} \leq \lambda_{PM}$, and $0 < \lambda_{Qm} \leq \lambda_{QM}$, where we denote by $\lambda_{Hm}$ and $\lambda_{HM}$ the minimum and the maximum eigenvalue, respectively, of a generic matrix $\mathbf{H} \in \mathbb{R}^{3\times 3}$. Next, let the scalar function

$$V = \boldsymbol{\xi}^T \mathbf{P}_\xi \boldsymbol{\xi} + \frac{1}{2}\boldsymbol{\eta}^T\boldsymbol{\eta} > 0\,, \tag{7.59}$$

satisfy the bounds

$$\lambda_{Vm}\|\boldsymbol{\zeta}\|^2 \leq V(\boldsymbol{\zeta}) \leq \lambda_{VM}\|\boldsymbol{\zeta}\|^2\,, \tag{7.60}$$

where $\lambda_{Vm} = \min\{1, \lambda_{Pm}\}$ and $\lambda_{VM} = \max\{1, \lambda_{PM}\}$. Define a region $B_\delta = \left\{\boldsymbol{\zeta} : \|\boldsymbol{\zeta}\| < \sqrt{\dfrac{\lambda_{Vm}}{\lambda_{VM}}} l_o\right\}$ and suppose that the initial condition satisfies $\boldsymbol{\zeta}(t_0) \in B_\delta$. Since $\dfrac{\lambda_{Vm}}{\lambda_{VM}} \leq 1$, $B_\delta$ is a subset of $B_r$.

By taking the time derivative of $V$ along the system trajectories, one obtains

$$\dot{V} = -(\dot{\gamma}_d + \eta_1)\boldsymbol{\xi}^T\mathbf{Q}_\xi\boldsymbol{\xi} + 2\boldsymbol{\xi}^T\mathbf{P}_\xi\mathbf{b}\eta_2 + \eta_1\dot{\eta}_1 + \eta_2\dot{\eta}_2\,, \tag{7.61}$$

where $\mathbf{b} = \begin{bmatrix} 0 & 0 & l_o c_\phi c_\psi \end{bmatrix}^T \in \mathbb{R}^3$. Taking into account (7.49) and (7.52) and the control law (7.56) yields

$$\dot{V} = -\dot{\gamma}_d \boldsymbol{\xi}^T \mathbf{Q}_\xi \boldsymbol{\xi} - \eta_1 \boldsymbol{\xi}^T \mathbf{Q}_\xi \boldsymbol{\xi} - k_{\eta 1}\eta_1^2 + 2\eta_2 \boldsymbol{\xi}^T \mathbf{P}_\xi \mathbf{b} - k_{\eta 2}\eta_2^2 \,. \tag{7.62}$$

Within the set $B_r$, this function can be upper bounded by

$$\begin{aligned}
\dot{V} \leq & -\dot{\gamma}_d \boldsymbol{\xi}^T \mathbf{Q}_\xi \boldsymbol{\xi} + \lambda_{QM} l_o^2 |\eta_1| - k_{\eta 1} |\eta_1|^2 \\
& + 2\lambda_{PM} l_o^2 |\eta_2| - k_{\eta 2} |\eta_2|^2 \\
\leq & -\dot{\gamma}_d \lambda_{Qm} \|\boldsymbol{\xi}\|^2 - |\eta_1| \left( k_{\eta 1} |\eta_1| - \lambda_{QM} l_o^2 \right) \\
& - |\eta_2| \left( k_{\eta 2} |\eta_2| - 2\lambda_{PM} l_o^2 \right) \\
= & -\dot{\gamma}_d \lambda_{Qm} \|\boldsymbol{\zeta}\|^2 - |\eta_1| \left( \left( k_{\eta 1} - \dot{\gamma}_d \lambda_{Qm} \right) |\eta_1| - \lambda_{QM} l_o^2 \right) \\
& - |\eta_2| \left( \left( k_{\eta 2} - \dot{\gamma}_d \lambda_{Qm} \right) |\eta_2| - 2\lambda_{PM} l_o^2 \right) \,,
\end{aligned} \tag{7.63}$$

since $\|\boldsymbol{\zeta}\|^2 = \|\boldsymbol{\xi}\|^2 + |\eta_1|^2 + |\eta_2|^2$. It can be noticed that the term

$$-|\eta_1| \left( \left( k_{\eta 1} - \dot{\gamma}_d \lambda_{Qm} \right) |\eta_1| - \lambda_{QM} l_o^2 \right) \tag{7.64}$$

is zero for $|\eta_1| = 0$ and negative for $|\eta_1| > \lambda_{QM} \dfrac{l_o^2}{k_{\eta 1} - \dot{\gamma}_d \lambda_{Qm}}$. Therefore, by continuity, a maximum for $|\eta_1|$ must exist. This maximum can be easily verified to be at $|\eta_1|_{max} = \lambda_{QM} \dfrac{l_o^2}{2\left(k_{\eta 1} - \dot{\gamma}_d \lambda_{Qm}\right)}$. Similar arguments can be used for the last term of (7.63). Overall, one has

$$\dot{V} \leq -\dot{\gamma}_d \lambda_{QM} \|\boldsymbol{\zeta}\|^2 + c_{\eta 1} + c_{\eta 2} \,, \tag{7.65}$$

where $c_{\eta 1} = \lambda_{QM}^2 \dfrac{l_o^4}{2\left(k_{\eta 1} - \dot{\gamma}_d \lambda_{Qm}\right)}$ and $c_{\eta 2} = 2\lambda_{PM}^2 \dfrac{l_o^4}{\left(k_{\eta 2} - \dot{\gamma}_d \lambda_{Qm}\right)}$, with $k_{\eta 1}, k_{\eta 2} > \dot{\gamma}_d \lambda_{Qm}$. Thus, it can be ensured that $\dot{V} \leq 0$ for

$$\|\boldsymbol{\zeta}\| \geq \sqrt{\frac{c_{\eta 1} + c_{\eta 2}}{\dot{\gamma}_d \lambda_{Qm}}} = \mu \,, \tag{7.66}$$

and the system trajectories are ultimately bounded by a region $B_\mu = \{\boldsymbol{\zeta} : \|\boldsymbol{\zeta}\| \leq \mu\}$. Because $k_{\eta 1}$ and $k_{\eta 2}$ can be chosen freely, the ultimate bound radius $\mu$ can be driven arbitrarily small. Moreover, $\mu$ can be easily forced to satisfy

$$\mu < \sqrt{\frac{\lambda_{Vm}}{\lambda_{VM}}} l_o \,, \tag{7.67}$$

to guarantee $B_\mu \subset B_r$.

There is a circularity in the proof[2]: when obtaining (7.63), it is implicitly assumed that $\boldsymbol{\zeta} \in B_r, \forall t \geq t_0$. To show that this is indeed the case, first notice that $\|\boldsymbol{\zeta}(t_0)\| \in B_\delta \implies \|\boldsymbol{\zeta}(t_0)\| < \sqrt{\dfrac{\lambda_{Vm}}{\lambda_{VM}}} l_o \leq l_o$. Suppose that $\boldsymbol{\zeta}$

[2] See [325], remarks on Theorem 5.3.1.

leaves $B_r$. By continuity, a time $T > t_0$ exists such that $\|\boldsymbol{\zeta}(T)\| = l_o$. Notice that, in order to leave $B_r$, the trajectories cannot enter in $B_\mu$ since this set is positively invariant because $\dot{V} \leq 0$ in its frontier. Therefore, the trajectories must remain within $B_r \backslash B_\mu$ before leaving $B_r$. On one hand, since $\dot{V} \leq 0$ for $t \in [t_0, T)$, and after (7.60)

$$V(\boldsymbol{\zeta}(T)) \leq V(\boldsymbol{\zeta}(t_0)) < \lambda_{Vm} l_o^2 \,. \tag{7.68}$$

On the other hand, from the assumption $\boldsymbol{\zeta}(T) = l_o$ and (7.60), one has

$$V(\boldsymbol{\zeta}(T)) = V(l_o) \geq \lambda_{Vm} l_o^2 \,. \tag{7.69}$$

By noticing that (7.68) and (7.69) are in contradiction, we can conclude that the original assumption is incorrect, and thus $\boldsymbol{\zeta}$ must remain in $B_r$. □

In the interior of $B_r$, taking into account (7.50) and (7.52), $\boldsymbol{\zeta} \approx \mathbf{0}$ implies $(z_o, \phi, \psi) \approx (z_{od}, 0, 0)$ and $\dot{\gamma} \approx \dot{\gamma}_d$, fulfilling the control objective. For simplicity, the upper-bound for the state $\boldsymbol{\zeta}$, which defines the region $B_r$ in Proposition 7.2.1, is chosen to be $l_o$. This choice makes the stability proof clearer, yet it is very conservative. However, since this bound is arbitrary, it can be modified to enlarge the controller's domain of attraction.

The next step is to design a control strategy to stabilise the pole dynamics. For this, it is assumed that the hoop has reached stationary state, such that $\ddot{\mathbf{q}}_o \equiv \mathbf{0}_2$. From (7.34a)–(7.34b) and (7.47) one has

$$\ddot{\mathbf{q}}_h = \mathbf{f}_h + \mathbf{f}_{uP} + \mathbf{Q}_o \mathbf{u}_Q \,, \tag{7.70}$$

where $\mathbf{f}_h = \mathbf{M}_h^{-1} \mathbf{c}_h \in \mathbb{R}^m$ and $\mathbf{f}_{uP} = \mathbf{P}_o \mathbf{u}_P \in \mathbb{R}^m$.

Investigating the controllability of the nonlinear system (7.70) is challenging, as discussed earlier. For this reason, only a local result is pursued, based on the linearisation of (7.70) around its nominal trajectory

$$\mathbf{q}^* = \left[\dot{\gamma}_d t \;\; 0 \;\; z_{od} \;\; (l_o/r_h)\dot{\gamma}_d t \;\; 0 \;\; \mathbf{q}_h^{*T}\right]^T , \tag{7.71}$$

$$\dot{\mathbf{q}}^* = \left[\dot{\gamma}_d \;\; 0 \;\; 0 \;\; (l_o/r_h)\dot{\gamma}_d \;\; 0 \;\; \dot{\mathbf{q}}_h^{*T}\right]^T , \tag{7.72}$$

where $\mathbf{q}_h^* \in \mathbb{R}^m$ is the vector representing the nominal trajectory for the pole. Only two of the study cases are analysed here: (i) $m = 3$, three Cartesian directions of movement along the $x_w$, $y_w$, and $z_w$ axes of $\mathcal{W}$[3] and (ii) $m = 4$, two Cartesian degree-of-freedom along $x_w$ and $y_w$ of $\mathcal{W}$, and two rotations around the same axes. The configuration coordinates for the three Cartesian degree-of-freedom case are the pole centre of mass coordinates $(o_{hx}, o_{hy}, o_{hz})$. For the latter case, the rotation matrix of the pole with respect to the inertial frame is given by the composition of two basic rotation matrices, namely

$$\mathbf{R}_o = \mathbf{R}_x(\alpha_1)\mathbf{R}_y(\alpha_2), \tag{7.73}$$

[3] This is the configuration studied in [117].

with $\alpha_1, \alpha_2 \in \mathbb{R}$ the rotation angles around $x_w$ and $y_w$, respectively, and $\mathbf{R}_x(\alpha_1), \mathbf{R}_y(\alpha_2) \in SO(3)$. Hence, the configuration coordinates for the pole are $(o_{hx}, o_{hy}, \alpha_1, \alpha_2)$ when $m = 4$. Therefore, the nominal trajectories for the pole in both cases are $\mathbf{q}_h^* = \dot{\mathbf{q}}_h^* = \mathbf{0}_m$.

Definined the state space coordinates $\mathbf{x} = \begin{bmatrix} \mathbf{q}_h^T & \dot{\mathbf{q}}_h^T \end{bmatrix}^T \in \mathbb{R}^{2m}$, the following linearised model can be obtained

$$\dot{\mathbf{x}} = \mathbf{A}(t)\mathbf{x} + \mathbf{B}(t)\mathbf{u}_Q \,, \tag{7.74}$$

where

$$\mathbf{A}(t) = \begin{bmatrix} \mathbf{O}_m & \mathbf{I}_m \\ \mathbf{A}_{21}(t) & \mathbf{A}_{22}(t) \end{bmatrix}, \tag{7.75}$$

$$\mathbf{B}(t) = \mathbf{Q}_o \Big|_{\mathbf{q}^*, \dot{\mathbf{q}}^*}, \tag{7.76}$$

$$\mathbf{a}_{21}(t) = \frac{\partial \mathbf{f}_h}{\partial \mathbf{q}_h} \Big|_{\mathbf{q}^*, \dot{\mathbf{q}}^*}, \tag{7.77}$$

$$\mathbf{a}_{22}(t) = \frac{\partial \mathbf{f}_h}{\partial \dot{\mathbf{q}}_h} \Big|_{\mathbf{q}^*, \dot{\mathbf{q}}^*}. \tag{7.78}$$

The term $\mathbf{f}_{uP}$ in (7.70) is considered as an external bounded input to carry out the linearisation. The periodic linear time-varying system (7.74) is *not controllable* [52, Theorem 6.11] when the three Cartesian inputrs are considered for the pole (*i.e.*, $m = 3$), while it is *controllable* [52, Theorem 6.12] when the two translations and the two rotations inputs are considered for the pole (*i.e.*, $m = 4$). For this last case, it is possible to find a stabilising controller of the form [280]

$$\mathbf{u}_Q = -\mathbf{\Gamma}^{-1}\mathbf{B}^T(t)\mathbf{R}(t)\mathbf{x} \,, \tag{7.79}$$

where $\mathbf{R}(t) \in \mathbb{R}^{8\times 8}$ is a symmetric positive definite time-varying matrix satisfying the Riccati equation

$$\dot{\mathbf{R}}(t) + \mathbf{A}^T(t)\mathbf{R}(t) + \mathbf{R}(t)\mathbf{A}(t) + \mathbf{G} = \mathbf{R}(t)\mathbf{B}(t)\mathbf{\Gamma}^{-1}\mathbf{B}^T(t)\mathbf{R}(t) \,, \tag{7.80}$$

with $\mathbf{G} \in \mathbb{R}^{8\times 8}$ and $\mathbf{\Gamma} \in \mathbb{R}^{4\times 4}$ two positive definite matrices of constant gains. By employing the *quasi–linearisation of the periodic Riccati equation* method [30, p. 137], an approximation for the solution of the Riccati equation (7.80) can be found.

#### 7.2.3.1 Conditions for maintaining contact

Rolling without slipping between the surfaces of the objects has been assumed for the modelling and control design presented in the above sections. Intuitively, it can be argued that there must be a minimal spinning speed for the hoop not to lose contact with the pole. For obtaining an approximation of the magnitude of this minimum speed, assume that stationary state has reached, *i.e.,* the hoop is spinning in the orthogonal plane to the main pole axis. The Lagrange multipliers from the Lagrange-d'Alembert formulation, which was used to obtain the model (7.34a)–(7.34b), can be employed to compute the internal forces [216, p. 279]. A direct calculation of the radial component gives the contact condition

$$m_o l_o \dot{\theta}^2 - m_o g > 0\,, \tag{7.81}$$

which represents the difference between the centripetal and gravity forces acting on the hoop. This minimum velocity is intended for the best scenario (the hoop perpendicular to the pole), thus the desired velocity and the initial conditions should satisfy $\dot{\theta} >> \sqrt{\frac{g}{l_o}}$. If the pole is in the vertical position, keeping the contact depends on the static friction between the surfaces. Hence, the desired and initial condition for the spinning speed must satisfy $\dot{\theta} >> \sqrt{\frac{g}{f_c l_o}}$, where $f_c > 0$ is the static friction coefficient. On the other hand, the upper limit for the spinning speed depends on the system's bandwidth, which is mainly limited by the signals acquisition and processing time and the actuators' maximum speed and acceleration. As an assumption for maintaining contact as well as to fulfil the requirements of Proposition 7.2.1, the desired hoop spinning velocity $\dot{\gamma}_d$ must be sufficiently close to the initial speed $\dot{\gamma}$, which in turn must be strictly greater than zero. The required swing controller to obtain this initial spinning is considered out of the scope of this paper, although some planar-motion open-loop controllers can induce it (*e.g.*, the one proposed in [278]).

### 7.2.4 Numerical simulation

A numerical simulation is carried out to test the validity of the proposed approach. The parameters employed for the simulation are listed in Table 7.2. The matrices and vectors in (7.34a)–(7.34b) were obtained through a symbolic computing software (*Wolfram Mathematica*) and are omitted here due to space constraints. It is assumed that the pole's apparent inertia can be assigned by the manipulator *e.g.,* as proposed in [95] for the pole not to be affected by the hoop motion. Notice that the pole's actual mass must not

have to be large, but only its apparent inertia. The pole sample time is considered to be $T = 0.005$ s, while the hoop coordinates are measured by means of a vision system with sample time $T_v = 0.02$ s.

Table 7.2: Simulation parameters

| Parameter | Value |
|---|---|
| $m_o$ | 0.05 kg |
| $m_h$ | 10 kg |
| $l_o$ | 0.3 m |
| $r_o$ | 0.005 m |
| $r_h$ | 0.025 m |
| $l_h$ | 0.7 m |

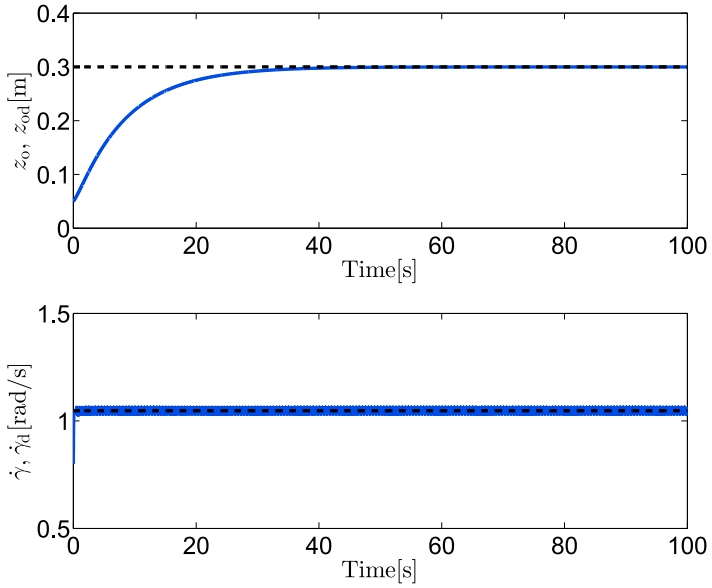


Fig. 7.2: Contact coordinates evolution: real (—), desired (- - -).

The desired references are $\dot{\gamma}_d = 4\dfrac{\pi r_h}{l_o} \approx 1.0472$ rad/s and $z_{od} = 0.3$ m. The gains for the LQR controller in (7.79)–(7.80) are chosen as $\mathbf{\Gamma} = diag\{0.5, 0.5, 1, 1\}$ and $\mathbf{G} = diag\{200, 200, 40000, 40000, 10, 10, 4, 4\}$. The hoop controller gains are chosen as $k_{\eta 1} = 20$, $k_{\eta 2} = 10$, $k_{\xi 1} = 40$, $k_{\xi 2} = 40$, and $k_{\xi 3} = 4$. The boundary condition for approximating $\mathbf{R}(t)$ is chosen as $\mathbf{R}(T_s) = \mathbf{O}_{8\times 8}$, where $T_s$ is the period of the linearised system (7.74), which

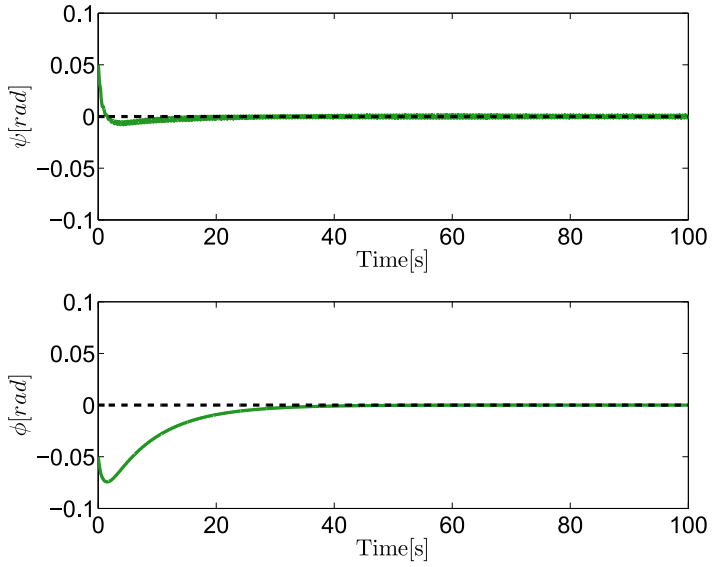


Fig. 7.3: Asymptotic stabilisation of the $\psi$ and $\phi$ coordinates.

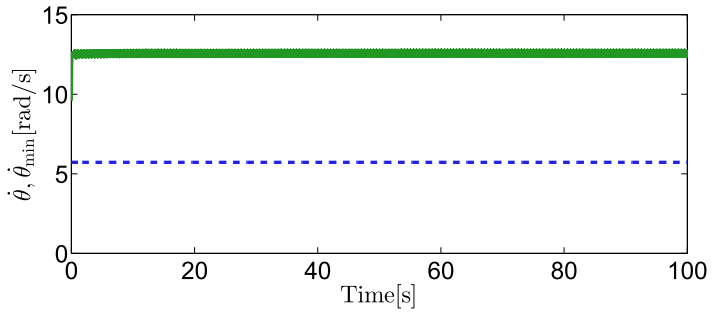


Fig. 7.4: Evolution of $\dot{\theta}$ (—) and the minimum value required to maintain contact (- - -).

is given by $T_s = \dfrac{l_o}{r_h}\dot{\gamma}_d$. The initial conditions for the generalised positions are set to $\gamma(t_0) = 0$ rad, $\psi(t_0) = 0.05$ rad, $z_o(t_0) = 0.05$ m, $\theta(t_0) = \pi$ rad, and $\phi(t_0) = -0.05$ rad, while the initial conditions for the velocities are set to $\dot{\gamma}(t_0) = 0.8$ rad/s, $\dot{\psi}(t_0) = 0$ rad/s, $\dot{z}_o(t_0) = -l_o \sin(\phi(t_0))\dot{\gamma}(t_0)$ m/s, $\dot{\theta}(t_0) = l_o \cos(\phi(t_0))\dfrac{\dot{\gamma}(t_0)}{r_h}$ rad/s, and $\dot{\phi}(t_0) = -\sin(\psi(t_0))\dot{\gamma}(t_0)$ rad/s.

The contact coordinates time evolution is shown in Fig. 7.2, where it can be seen that the control objective is satisfied. In Fig. 7.3, the graphs of the $\psi$ and $\phi$ coordinates are displayed, showing their ultimate boundedness within a

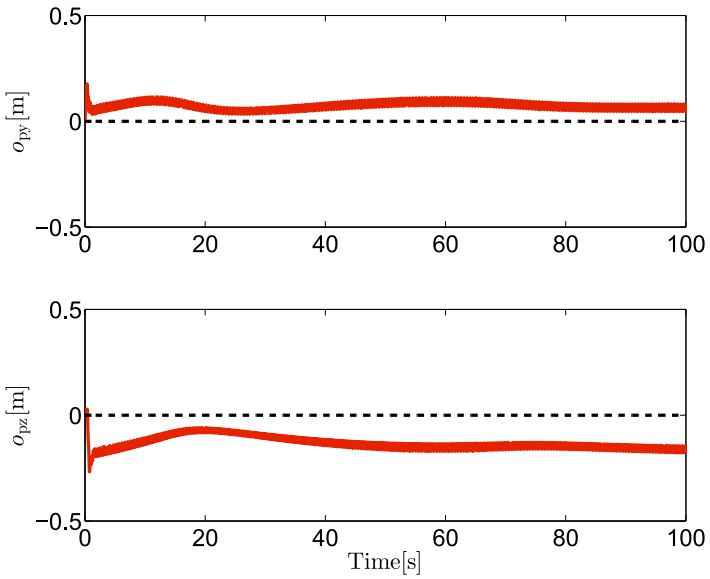


Fig. 7.5: Pole's Cartesian coordinates with respect to the initial position.

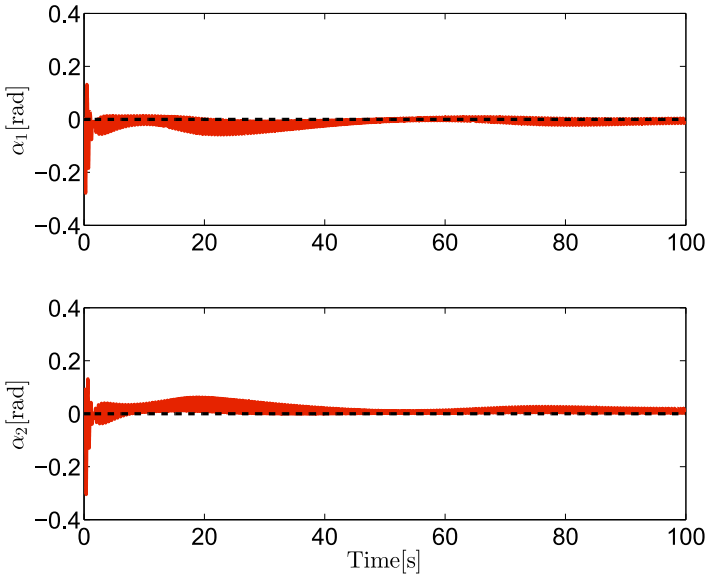


Fig. 7.6: Stabilisation of the pole's rotation angles.

small region around the origin. The $\dot{\theta}$ coordinate time evolution is displayed in Fig. 7.4, along with the minimum speed required to maintain contact.

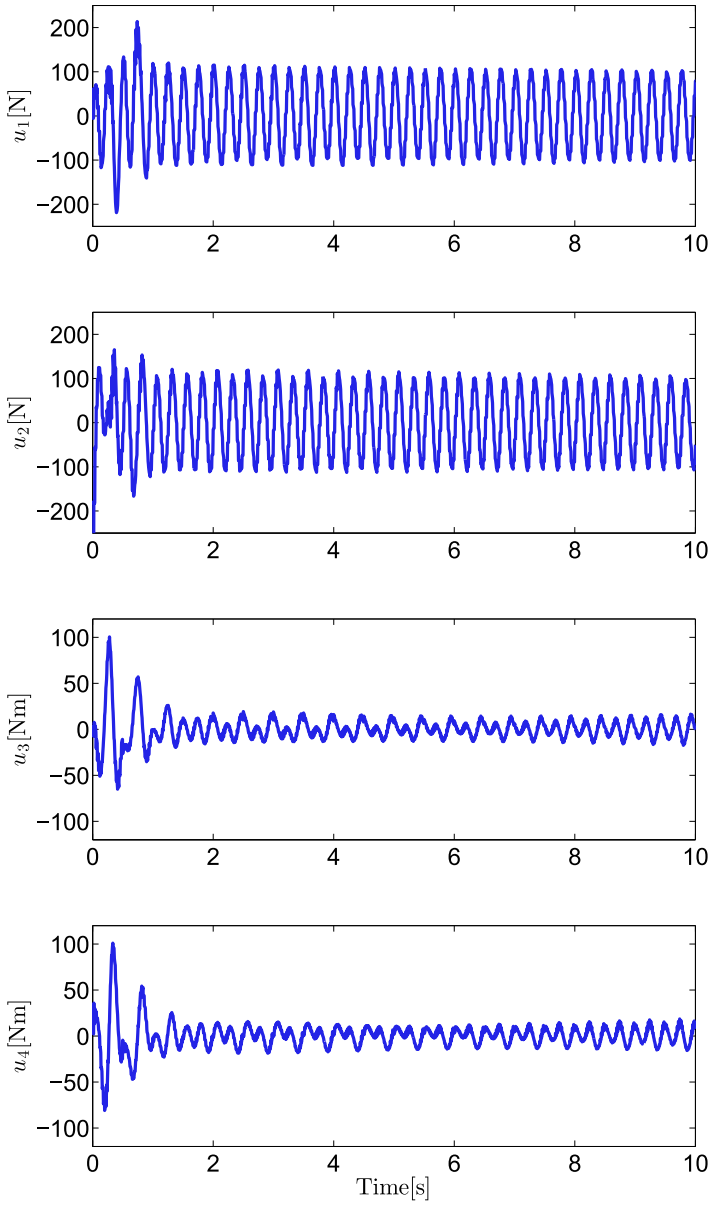


Fig. 7.7: Force and torque inputs on the pole.

This condition is satisfied during all the simulation time with a considerably large margin. The Cartesian coordinates of the pole centre of mass are shown in Fig. 7.5, while the time evolution of the two angles describing the pole

orientation is shown in Fig. 7.6. It can be seen that the proposed controller stabilises all the pole coordinates. Finally, the control inputs, *i.e.*, the forces and torques acting on the pole, for the first 10 seconds of the simulation are shown in Figure 7.7.

## 7.3 Ballbot

Contemporary research on robotics has steered towards the incorporation of robots into the everyday lives of humans. Robots are expected to interact with humans both outdoors and in human environments safely. This motivation requires robots not only to be mobile and slim but also tall enough to facilitate interaction. On the other hand, conventional multi-wheeled statically-stable robots are typically built to have a low center of gravity to prevent them from easily tipping over. The satisfaction of these two conflicting requirements urges the mobile robots to have large, wide, and heavy bases. At the cost of designing a more complicated controller, a more efficient method to tackle the interaction problem is to utilize dynamically stable robots.

One of the most popular dynamically balancing robots is the two-wheeled Segway [226]. The ballbot was introduced as a mobile robot moving on a single spherical omnidirectional wheel [164, 165]. The ballbot, whose design is detailed in [220, 218], is typically slim and as tall as an adult human, rendering it able to interact with humans while navigating constrained environments.

Even though a variant of this robot has been built by many laboratories [128, 168], its control framework has been restricted to the use of classic methods such as linearization about the desired equilibrium in coordinates and PID controllers [168, 157]. Derivation of the equations of motion of the ballbot with a 3-DoF manipulator mounted on top using both Lagrange's and Kane's methods have been performed in [9]. The authors have confirmed that the two approaches agree with each other with a numerical simulation. They have also designed two control laws for the planar motion of the ballbot and manipulation, respectively, without explicitly addressing stability properties. Moreover, many controllers are typically developed by restricting the dynamics of the ballbot to a vertical 2D plane and applied to the 3D robot by an *ad-hoc* extension to two distinct vertical planes. This procedure inevitably ignores the energetic interaction of the full dynamics of the robot along these planes. Trajectory planning based on motion primitives has been presented in [217], while in [219], authors plan a trajectory for the ballbot equipped with right and left arms. A sliding-mode controller has also been designed for this system in [170]. For the most part, the equations of motion of the whole dynamics of the ballbot have been derived in coordinates, which injects a fair bit of unnecessary complexity into the problem formulation, requires the use of symbolic manipulation software and a decent amount of storage space in the computer [168]. The only exception to this trend has been provided

in [138], where the authors derive a dynamic model of the ballbot, which additionally assumes that the body has no yaw motion relative to the ball using Newton's laws. This lengthy procedure, which was omitted from the chapter due to space considerations, leads to a dynamical model of the system, which is not particularly easy to work with for control synthesis. Lastly, in [163], a stabilization algorithm for a TWMM, which is a robot with similar characteristics to the ballbot, has been presented. The controller designed in this chapter utilizes the ZMP idea from the bipedal robotic literature to asymptotically stabilize the motion of the TWMM.

In this chapter, we derive the Euler-Lagrange equations of motion of the full dynamics of the ballbot without resort to any coordinate system. This yields a compact, yet explicit representation of the equations of motion, which recover the 2D dynamics of the ballbot, restricted to a vertical plane, given in the literature [218]. Preliminary results on the derivation and linearization of the intrinsic dynamics of the ballbot are reported in [270]. The Euler-Poincaré dynamics developed in this chapter yield a reduced set of 10 first-order ODEs that govern the motion of the ballbot as opposed to the conventional Newton-Euler approach, which would yield 16 first-order ODEs. We develop energy-shaping control laws that use the available control inputs to make the system look like a new Lagrangian system with a desired asymptotically stable equilibrium point for both the 2D and the 3D dynamics of the ballbot. While in the 2D case we can follow the procedure outlined in [81] to shape the energy, this procedure needs to be extended for the 3D-case because the form of the Euler-Poincaré does not precisely match the form of the Euler-Lagrange equations as handled in that work. The derivation of the total energy shaping control law for the ballbot shows the approach's applicability to a system with considerably more states than the examples previously reported in the literature. The main contribution of this chapter is providing an intrinsic and unified framework to study dynamics and control of the balancing system consisting of a heavy top on a spherical wheel and providing nonlinear energy-shaping control law whose basin of attraction is almost global as long as the mechanism is judiciously designed.

### 7.3.1 Lagrangian dynamics of the ballbot

In this section, we present the background information to be used in the remainder of this chapter, including the kinematics and dynamics of the ballbot. We start by noting that every vector quantity in this paper is represented in the spatial world frame $\mathcal{W}$.

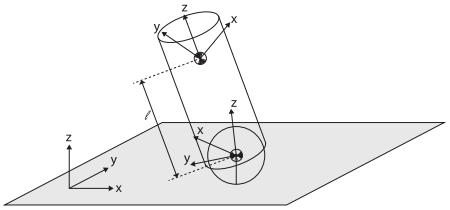


Fig. 7.8: Ballbot: bodies and frames

#### 7.3.1.1 Background and kinematics

The skeleton diagram of the ballbot is depicted in Figure 7.8. It is constructed via the interconnection of a rigid spherical wheel and a rigid cylindrical body. The body is unable to translate with respect to the ball but is free to move otherwise. Therefore, the configuration manifold of the ballbot is $Q = \mathbb{R}^2 \times SO(3) \times SO(3)$. The world inertial frame $\mathcal{W}$ is fixed to a horizontal plane. The spherical wheel is represented by the frame $\mathcal{H}$ and is assumed to have its center of mass at its geometric center. As a result, the vector from the point of contact of the ball with the ground and its center of mass is given by $r_h \mathbf{e}_3$ in the inertial frame. The cylindrical rigid body situated on the wheel is referred to as the "top," and it is denoted by the reference frame $\mathcal{O}$. The center of mass of the top is assumed to lie on the central axis of its geometrical shape at a distance $l$ from the center of the ball. The ball is assumed to roll without slipping, yielding the well-known nonholonomic constraint between the time derivative of its position vector $\mathbf{p}_{sb}$ and its spatial angular velocity $\boldsymbol{\omega}_{sb}$

$$\dot{\mathbf{p}}_{sb} = r_h \boldsymbol{\omega}_{sb} \times \mathbf{e}_3 = r_h \hat{\boldsymbol{\omega}}_{sb} \mathbf{e}_3, \tag{7.82}$$

where we introduced the *hat* $\wedge$ operator, which stands for the standard isomorphism between $\mathbb{R}^3$ and $\mathfrak{so}(3)$. Its inverse is denoted by the symbol $\vee$, known as the *vee* map [216].

The kinematics of the orientation of the ball and the top are given in the frame $\mathcal{W}$ by the familiar rigid body orientation kinematics

$$\dot{\mathbf{R}}_{sb} = \hat{\boldsymbol{\omega}}_{sb} \mathbf{R}_{sb}, \quad \dot{\mathbf{R}}_{st} = \hat{\boldsymbol{\omega}}_{st} \mathbf{R}_{st}. \tag{7.83}$$

Using notation and methods from [216], we express the velocity of the top with respect to the inertial frame $\mathbf{V}_{st} \in \mathbb{R}^6$ in terms of the velocity of the ball with respect to the inertial frame $\mathbf{V}_{sb} \in \mathbb{R}^6$ and the velocity of the top with respect to the ball $\mathbf{V}_{bt} \in \mathbb{R}^6$

$$\mathbf{V}_{st} = \begin{bmatrix} \mathbf{v}_{st} \\ \boldsymbol{\omega}_{st} \end{bmatrix} = \begin{bmatrix} \mathbf{v}_{sb} + \mathbf{p}_{sb} \times \mathbf{R}_{sb} \boldsymbol{\omega}_{bt} \\ \boldsymbol{\omega}_{sb} + \mathbf{R}_{sb} \boldsymbol{\omega}_{bt} \end{bmatrix}. \tag{7.84}$$

We can now compute the time derivative of $\mathbf{p}_{st}$ as a function of the time derivative of $\mathbf{p}_{sb}$, the angular velocity of the top with respect to $\mathcal{W}$ and the orientation of the top:

$$\dot{\mathbf{p}}_{st} = \dot{\mathbf{p}}_{sb} + l\boldsymbol{\omega}_{st} \times \mathbf{R}_{st}\mathbf{e}_3. \tag{7.85}$$

Throughout this chapter, some properties of the hat map that we freely use in the remainder are as follows

$$\begin{aligned} \hat{\mathbf{x}}\mathbf{y} &= \mathbf{x} \times \mathbf{y} = -\mathbf{y} \times \mathbf{x} = -\hat{\mathbf{y}}\mathbf{x}, \\ \mathbf{x}^T\hat{\mathbf{y}}\mathbf{z} &= \mathbf{y}^T\hat{\mathbf{z}}\mathbf{x} = \mathbf{z}^T\hat{\mathbf{x}}\mathbf{y}, \\ \hat{\mathbf{x}}\hat{\mathbf{y}}\hat{\mathbf{z}} &= \left(\mathbf{x}^T\mathbf{z}\right)\mathbf{y} - \left(\mathbf{x}^T\mathbf{y}\right)\mathbf{z}, \end{aligned}$$

for any $\mathbf{x}, \mathbf{y}, \mathbf{z} \in \mathbb{R}^3$.

#### 7.3.1.2 Lagrangian

We write the Lagrangian of the ballbot in $\mathcal{W}$, that is, as seen by an observer stationary in the inertial frame. Note that it is imperative that the rolling constraint (7.82) not be inserted into the Lagrangian before its variation is taken. Suppose the variation of the Lagrangian is taken after the substitution of the nonholonomic constraints. In that case, this yields the vakonomic equations, which disagree with the dynamics of rigid bodies. Instead, one should take the variation before the imposition of the nonholonomic constraints, leading to the Lagrange-d'Alembert equations, the correct equations of motion [169, 11].

The kinetic energy of the ball, $K_b \in \mathbb{R}$, is given by the sum of its rotational and translational kinetic energies, while its potential energy, $V_b \in \mathbb{R}$, is zero, since its height with respect to the inertial frame remains a constant

$$\begin{aligned} K_b &= \frac{1}{2}\boldsymbol{\omega}_{sb}^T\mathbf{I}_b\boldsymbol{\omega}_{sb} + \frac{1}{2}m_b\dot{\mathbf{p}}_{sb}^T\dot{\mathbf{p}}_{sb}, \\ V_b &= 0. \end{aligned}$$

The potential energy of the top, $V_t \in \mathbb{R}$, is given by the height of its center of mass from the horizontal multiplied by its mass. The kinetic energy of the top, $K_t \in \mathbb{R}$, can be written in terms of the rotational velocity of the top and the translational velocity of the ball with respect to $\mathcal{W}$ by substituting from (7.85):

$$\begin{aligned} K_t &= \frac{1}{2}\boldsymbol{\omega}_{st}^T\mathbf{I}_t\boldsymbol{\omega}_{st} + \frac{1}{2}m_t\dot{\mathbf{p}}_{st}^T\dot{\mathbf{p}}_{st}^T \\ &= \frac{1}{2}\boldsymbol{\omega}_{st}^T\mathbf{I}_t\boldsymbol{\omega}_{st} + \frac{1}{2}m_t l^2\boldsymbol{\omega}_{st}^T\boldsymbol{\omega}_{st} + \frac{1}{2}m_t\dot{\mathbf{p}}_{sb}^T\dot{\mathbf{p}}_{sb} \\ &\quad - \frac{1}{2}m_t l^2\left(\boldsymbol{\omega}_{st}^T\mathbf{R}_{st}\mathbf{e}_3\right)^2 + m_t l\dot{\mathbf{p}}_{sb}^T\left(\boldsymbol{\omega}_{st} \times \mathbf{R}_{st}\mathbf{e}_3\right), \end{aligned}$$

$$V_t = m_t g l \mathbf{e}_3^T \mathbf{R}_{st} \mathbf{e}_3.$$

Therefore, the Lagrangian $L = K - V = K_t + K_b - V_t \in \mathbb{R}$ is

$$\begin{aligned} L = &\frac{1}{2}\boldsymbol{\omega}_{st}^T \mathbf{I}_t \boldsymbol{\omega}_{st} + \frac{1}{2} m_t l^2 \boldsymbol{\omega}_{st}^T \boldsymbol{\omega}_{st} + \frac{1}{2}\boldsymbol{\omega}_{sb}^T \mathbf{I}_b \boldsymbol{\omega}_{sb} + \frac{1}{2}(m_b + m_t)\dot{\mathbf{p}}_{sb}^T \dot{\mathbf{p}}_{sb} \\ &- \frac{1}{2} m_t l^2 \left(\boldsymbol{\omega}_{st}^T \mathbf{R}_{st} \mathbf{e}_3\right)^2 + m_t l \dot{\mathbf{p}}_{sb}^T \left(\boldsymbol{\omega}_{st} \times \mathbf{R}_{st} \mathbf{e}_3\right) - m_t g l \mathbf{e}_3^T \mathbf{R}_{st} \mathbf{e}_3. \end{aligned} \tag{7.86}$$

Let us define an element of the unit 2-sphere $\boldsymbol{\gamma} := \mathbf{R}_{st}\mathbf{e}_3$. This quantity represents the direction of the center of mass of the top expressed in $\mathcal{W}$. Next, we write the Lagrangian in terms of $\boldsymbol{\gamma}$, the angular velocity of the top with respect to $\mathcal{W}$ and the angular velocity of the ball with respect to $\mathcal{O}$, all expressed in $\mathcal{W}$. We represent the latter quantity by $\bar{\boldsymbol{\omega}}_{tb} \in \mathbb{R}^3$ and compute it by $\bar{\boldsymbol{\omega}}_{tb} = \boldsymbol{\omega}_{sb} - \boldsymbol{\omega}_{st}$. When the Lagrangian (7.86) is expressed with these quantities, it takes the reduced form

$$\begin{aligned} \ell = &\frac{1}{2}\left\langle \boldsymbol{\omega}_{st}, \left(\mathbf{I}_t + \mathbf{I}_b + m_t l^2 \mathbf{I}_3\right)\boldsymbol{\omega}_{st}\right\rangle + \left\langle \boldsymbol{\omega}_{st}, \mathbf{I}_b \bar{\boldsymbol{\omega}}_{tb}\right\rangle \\ &+ \frac{1}{2}\left\langle \bar{\boldsymbol{\omega}}_{tb}, \mathbf{I}_b \bar{\boldsymbol{\omega}}_{tb}\right\rangle + \frac{1}{2}(m_b + m_t)\left\langle \dot{\mathbf{p}}_{sb}, \dot{\mathbf{p}}_{sb}\right\rangle \\ &- \frac{1}{2} m_t l^2 \left\langle \boldsymbol{\omega}_{st}, \boldsymbol{\gamma}\right\rangle^2 + m_t l \left\langle \dot{\mathbf{p}}_{sb}, \boldsymbol{\omega}_{st} \times \boldsymbol{\gamma}\right\rangle - m_t g l \left\langle \mathbf{e}_3, \boldsymbol{\gamma}\right\rangle. \end{aligned} \tag{7.87}$$

#### 7.3.1.3 Euler-Poincaré equations of the ballbot

The equations of motion of the ballbot can be reduced from $TQ$ to $\mathfrak{so}(3) \times \mathfrak{so}(3) \times \mathbb{S}^2 \times \mathbb{R}^2$ to yield the Euler-Poincaré equations [273] for the ballbot. We can derive the evolution of $\boldsymbol{\gamma}$ by differentiating its definition and using the kinematics of the rigid body

$$\dot{\boldsymbol{\gamma}} = \dot{\mathbf{R}}_{st}\mathbf{e}_3 = \boldsymbol{\omega}_{st} \times \mathbf{R}_{st}\mathbf{e}_3 = \boldsymbol{\omega}_{st} \times \boldsymbol{\gamma}, \tag{7.88a}$$

$$\dot{\boldsymbol{\gamma}} + \boldsymbol{\gamma} \times \boldsymbol{\omega}_{st} = \mathbf{0_3}. \tag{7.88b}$$

We freely make use of the following identities when taking the variation of the reduced Lagrangian (7.87):

$$\delta \mathbf{R}^{-1} = -\mathbf{R}^{-1}\delta\mathbf{R}\mathbf{R}^{-1}, \tag{7.89a}$$

$$\delta \mathbf{I} = \delta\mathbf{R}\mathbf{R}^{-1}\mathbf{I} - \mathbf{I}\delta\mathbf{R}\mathbf{R}^{-1}, \tag{7.89b}$$

$$\delta\boldsymbol{\omega} = \dot{\boldsymbol{\eta}} + \boldsymbol{\eta} \times \boldsymbol{\omega}, \tag{7.89c}$$

$$\delta\dot{\mathbf{p}} = \frac{\mathrm{d}}{\mathrm{d}t}\left(\delta\mathbf{p}\right). \tag{7.89d}$$

where $\mathbf{R} \in SO(3)$, $\boldsymbol{\omega} \in \mathfrak{so}(3)$, $\mathbf{p} \in \mathbb{R}^3$, and $\mathfrak{so}(3) \ni \hat{\boldsymbol{\eta}} = \delta\mathbf{R}\mathbf{R}^{-1}$ are generic element.

The action integral is given by $s = \int \ell \, \mathrm{d}t$, whose variation, $\delta s = \int \delta\ell \, \mathrm{d}t$ is computed by

$$\delta s = \int \left( \frac{\delta \ell}{\delta \mathbf{R}_{st}} \delta \mathbf{R}_{st} + \frac{\delta \ell}{\delta \boldsymbol{\omega}_{st}} \delta \boldsymbol{\omega}_{st} + \frac{\delta \ell}{\delta \bar{\boldsymbol{\omega}}_{tb}} \delta \bar{\boldsymbol{\omega}}_{tb} + \frac{\delta \ell}{\delta \boldsymbol{\gamma}} \delta \boldsymbol{\gamma} + \frac{\delta \ell}{\delta \dot{\mathbf{p}}_{sb}} \delta \dot{\mathbf{p}}_{sb} \right) \mathrm{d}t.$$

Let us compute the individual terms of the above expression making use of the additional relation $\delta\boldsymbol{\gamma} = \boldsymbol{\eta}_{st} \times \boldsymbol{\gamma}$

$$\begin{aligned}
\int \frac{\delta \ell}{\delta \mathbf{R}_{st}} \delta \mathbf{R}_{st} \, \mathrm{d}t \; &= \int \frac{1}{2} \left\langle \boldsymbol{\omega}_{st}, \left( \hat{\boldsymbol{\eta}}_{st} \mathbf{I}_t - \mathbf{I}_t \hat{\boldsymbol{\eta}}_{st} \right) \boldsymbol{\omega}_{st} \right\rangle \mathrm{d}t = \int \left\langle \mathbf{I}_t \boldsymbol{\omega}_{st} \times \boldsymbol{\omega}_{st}, \boldsymbol{\eta}_{st} \right\rangle \mathrm{d}t, \\
\int \frac{\delta \ell}{\delta \boldsymbol{\omega}_{st}} \delta \boldsymbol{\omega}_{st} \, \mathrm{d}t &= \int \left\langle \frac{\partial \ell}{\partial \boldsymbol{\omega}_{st}}, \dot{\boldsymbol{\eta}}_{st} + \boldsymbol{\eta}_{st} \times \boldsymbol{\omega}_{st} \right\rangle \mathrm{d}t \\
&= \int \left\{ \left\langle -\frac{\mathrm{d}}{\mathrm{d}t} \frac{\partial \ell}{\partial \boldsymbol{\omega}_{st}} + \boldsymbol{\omega}_{st} \times \frac{\partial \ell}{\partial \boldsymbol{\omega}_{st}}, \boldsymbol{\eta}_{st} \right\rangle \right\} \mathrm{d}t \\
&= \int \Big\langle - \left( \hat{\boldsymbol{\omega}}_{st} \mathbf{I}_t - \mathbf{I}_t \hat{\boldsymbol{\omega}}_{st} \right) \boldsymbol{\omega}_{st} - \left( \mathbf{I}_t + \mathbf{I}_b + m_t l^2 \mathbf{I}_3 \right) \dot{\boldsymbol{\omega}}_{st} - \mathbf{I}_b \dot{\bar{\boldsymbol{\omega}}}_{tb} \\
&\qquad + m_t l^2 \left( \langle \dot{\boldsymbol{\omega}}_{st}, \boldsymbol{\gamma} \rangle \boldsymbol{\gamma} + \langle \boldsymbol{\omega}_{st}, \boldsymbol{\gamma} \rangle \boldsymbol{\omega}_{st} \times \boldsymbol{\gamma} \right) \\
&\qquad - m_t l \left( \left( \boldsymbol{\omega}_{st} \times \boldsymbol{\gamma} \right) \times \dot{\mathbf{p}}_{sb} + \boldsymbol{\gamma} \times \ddot{\mathbf{p}}_{sb} \right) + \boldsymbol{\omega}_{st} \\
&\qquad \times \left( \mathbf{I}_t + \mathbf{I}_b + m_t l^2 \mathbf{I}_3 \right) \boldsymbol{\omega}_{st} + \boldsymbol{\omega}_{st} \times \mathbf{I}_b \bar{\boldsymbol{\omega}}_{tb} - m_t l^2 \left\langle \boldsymbol{\omega}_{st}, \boldsymbol{\gamma} \right\rangle \boldsymbol{\omega}_{st} \\
&\qquad \times \boldsymbol{\gamma} + m_t l \left( \boldsymbol{\omega}_{st} \times \left( \boldsymbol{\gamma} \times \dot{\mathbf{p}}_{sb} \right) \right), \boldsymbol{\eta}_{st} \Big\rangle \, \mathrm{d}t, \\
\int \frac{\delta \ell}{\delta \bar{\boldsymbol{\omega}}_{tb}} \delta \bar{\boldsymbol{\omega}}_{tb} \, \mathrm{d}t &= \int \langle - \frac{\mathrm{d}}{\mathrm{d}t} \frac{\partial \ell}{\partial \bar{\boldsymbol{\omega}}_{tb}} + \bar{\boldsymbol{\omega}}_{tb} \times \frac{\partial \ell}{\partial \bar{\boldsymbol{\omega}}_{tb}} \rangle \, \mathrm{d}t \\
&= \int \left\langle -\mathbf{I}_b \left( \dot{\boldsymbol{\omega}}_{st} + \dot{\bar{\boldsymbol{\omega}}}_{tb} \right) + \bar{\boldsymbol{\omega}}_{tb} \times \mathbf{I}_b \left( \boldsymbol{\omega}_{st} + \bar{\boldsymbol{\omega}}_{tb} \right), \bar{\boldsymbol{\eta}}_{tb} \right\rangle \mathrm{d}t, \\
\int \frac{\delta \ell}{\delta \boldsymbol{\gamma}} \delta \boldsymbol{\gamma} \, \mathrm{d}t \; &= \int \left\langle \frac{\partial \ell}{\partial \boldsymbol{\gamma}}, \boldsymbol{\eta}_{st} \times \boldsymbol{\gamma} \right\rangle \mathrm{d}t = \int \left\langle \boldsymbol{\gamma} \times \frac{\partial \ell}{\partial \boldsymbol{\gamma}}, \boldsymbol{\eta}_{st} \right\rangle \mathrm{d}t \\
&= \int \left\langle -m_t l^2 \langle \boldsymbol{\omega}_{st}, \boldsymbol{\gamma} \rangle \boldsymbol{\gamma} \times \boldsymbol{\omega}_{st} + m_t l \left( \boldsymbol{\gamma} \times \left( \dot{\mathbf{p}}_{sb} \times \boldsymbol{\omega}_{st} \right) \right) - m_t g l \boldsymbol{\gamma} \times \mathbf{e}_3, \boldsymbol{\eta}_{st} \right\rangle \mathrm{d}t, \\
\int \frac{\delta \ell}{\delta \dot{\mathbf{p}}_{sb}} \delta \dot{\mathbf{p}}_{sb} \, \mathrm{d}t &= \int \langle - \frac{\mathrm{d}}{\mathrm{d}t} \frac{\partial \ell}{\partial \dot{\mathbf{p}}_{sb}}, \delta \mathbf{p}_{sb} \rangle \, \mathrm{d}t \\
&= \int \langle -(m_b + m_t) \ddot{\mathbf{p}}_{sb} - m_t l \left( \dot{\boldsymbol{\omega}}_{st} \times \boldsymbol{\gamma} + \boldsymbol{\omega}_{st} \times \left( \boldsymbol{\omega}_{st} \times \boldsymbol{\gamma} \right) \right), \delta \mathbf{p}_{sb} \rangle \, \mathrm{d}t \\
&= \int \langle -(m_b + m_t) r_h \ddot{\mathbf{p}}_{sb} \\
&\qquad - m_t l \left( \dot{\boldsymbol{\omega}}_{st} \times \boldsymbol{\gamma} + \boldsymbol{\omega}_{st} \times \left( \boldsymbol{\omega}_{st} \times \boldsymbol{\gamma} \right) \right), \left( \boldsymbol{\eta}_{st} + \bar{\boldsymbol{\eta}}_{tb} \right) \times \mathbf{e}_3 \rangle \, \mathrm{d}t \\
&= \int \langle -(m_b + m_t) r_h \mathbf{e}_3 \times \ddot{\mathbf{p}}_{sb} - m_t r_h l \left( \mathbf{e}_3 \times \left( \dot{\boldsymbol{\omega}}_{st} \times \boldsymbol{\gamma} \right) + \mathbf{e}_3 \right. \\
&\qquad \left. \times \left( \boldsymbol{\omega}_{st} \times \left( \boldsymbol{\omega}_{st} \times \boldsymbol{\gamma} \right) \right) \right), \left( \boldsymbol{\eta}_{st} + \bar{\boldsymbol{\eta}}_{tb} \right) \rangle \, \mathrm{d}t.
\end{aligned}$$

Keeping accordance with the literature, we assume that the rotation of the ball along the $z$-axis of $\mathcal{W}$ cannot be actuated and is always a constant during the motion of the ballbot. We consider the scenario where the relative

orientation between the ball and the top is actuated as in [218, 168]. In other words, the control input belongs to the subbundle of the cotangent bundle of $Q$, characterized by the annihilator of the relative angular velocity $\boldsymbol{\omega}_{tb}$: $\boldsymbol{\tau}' \in \{\boldsymbol{\sigma} \in \mathfrak{so}^*(3) : \langle \boldsymbol{\sigma}, \boldsymbol{\omega}_{tb} \rangle = 0\}$, after its identification with $\mathbb{R}^3$. We notice that $\hat{\boldsymbol{\omega}}_{tb} = \mathrm{Ad}_{\mathbf{R}_{st}^T}(\hat{\boldsymbol{\omega}}_{sb} - \hat{\boldsymbol{\omega}}_{st})$, where Ad is the adjoint action, and using the dual of this mapping, we find the forced Euler-Lagrange equations of motion of the ballbot. We add the variations computed above and insert the rolling constraint (7.82) expressed as $\dot{\mathbf{p}}_{sb} = r\,(\boldsymbol{\omega}_{st} + \bar{\boldsymbol{\omega}}_{tb}) \times \mathbf{e}_3$ to arrive at

$$\begin{aligned}
&\big(\mathbf{I}_t + m_t l^2\left(\mathbf{I}_3 - \boldsymbol{\gamma}\otimes\boldsymbol{\gamma}^T\right) + \mathbf{I}_b \\
&\quad - (m_b+m_t) r_h^2 \hat{\mathbf{e}}_3^2 - m_t r_h l\left(\hat{\boldsymbol{\gamma}}\hat{\mathbf{e}}_3 + \hat{\mathbf{e}}_3\hat{\boldsymbol{\gamma}}\right)\big)\,\dot{\boldsymbol{\omega}}_{st} \\
&\quad + \Big(\mathbf{I}_b - (m_b+m_t) r_h^2 \hat{b f e}_3^2 - m_t r_h l \hat{\boldsymbol{\gamma}}\hat{\mathbf{e}}_3\Big)\,\dot{\bar{\boldsymbol{\omega}}}_{tb} + m_t l^2 \langle \boldsymbol{\omega}_{st}, \boldsymbol{\gamma}\rangle\,\hat{\boldsymbol{\gamma}}\boldsymbol{\omega}_{st} \\
&\quad + m_t r_h l \hat{\mathbf{e}}_3 \hat{\boldsymbol{\omega}}_{st}^2 \boldsymbol{\gamma} + \boldsymbol{\omega}_{st} \times \mathbf{I}_t \boldsymbol{\omega}_{st} - \boldsymbol{\omega}_{st} \times \mathbf{I}_b \bar{\boldsymbol{\omega}}_{tb} - m_t g l \mathbf{e}_3 \times \boldsymbol{\gamma} = \mathbf{0_3},
\end{aligned} \tag{7.90a}$$

$$\begin{aligned}
&\left(\mathbf{I}_b - (m_b+m_t) r_h^2 \hat{\mathbf{e}}_3^2 - m_t r_h l \hat{\mathbf{e}}_3 \hat{\boldsymbol{\gamma}}\right)\dot{\boldsymbol{\omega}}_{st} \\
&\quad + \left(\mathbf{I_b} - (\mathbf{m_b}+\mathbf{m_t})\mathbf{r_h^2}\hat{\mathbf{e}}_3^2\right)\dot{\bar{\boldsymbol{\omega}}}_{tb} \\
&\quad + m_t r_h l \hat{\mathbf{e}}_3 \hat{\boldsymbol{\omega}}_{st}^2 \boldsymbol{\gamma} - \bar{\boldsymbol{\omega}}_{tb} \times \mathbf{I}_b \boldsymbol{\omega}_{st} = \mathbf{R}_{st}\boldsymbol{\tau},
\end{aligned} \tag{7.90b}$$

with $\boldsymbol{\tau} \in \mathbb{R}^3$ the control input. Notice that this system is defined on $\mathfrak{so}(3) \times \mathfrak{so}(3) \times \mathbb{S}^2 \times \mathbb{R}^2$, which has dimension 10, as opposed to the original system, which is defined on $TQ$, with a dimension count of 16. In case the translational dynamics of the ball, which does not affect the stability of the system, is not considered, the reduced equations evolve on an 8-dimensional manifold, whereas the original equations of motion evolve on a 12-dimensional one.

We note the following definitions to be utilized as in the subsequent sections:

$$\begin{aligned}
\mathbf{M}_{11} &= \mathbf{I}_t + m_t l^2\left(\mathbf{I}_3 - \boldsymbol{\gamma}\otimes\boldsymbol{\gamma}^T\right) + \mathbf{I}_b - (m_b+m_t) r_h^2 \hat{\mathbf{e}}_3^2 - m_t r_h l\left(\hat{\boldsymbol{\gamma}}\hat{\mathbf{e}}_3 + \hat{\mathbf{e}}_3\hat{\boldsymbol{\gamma}}\right), \\
\mathbf{M}_{12} &= \mathbf{I}_b - (m_b+m_t) r_h^2 \hat{\mathbf{e}}_3^2 - m_t r_h l \hat{\boldsymbol{\gamma}}\hat{\mathbf{e}}_3, \\
\mathbf{M}_{22} &= \mathbf{I}_b - (m_b+m_t) r_h^2 \hat{\mathbf{e}}_3^2.
\end{aligned}$$

A comparison of the Euler-Poincaré dynamics and the conventional Euler-Lagrange equations derived using coordinates is made in Figure 7.9, where the errors in $\mathbf{R}_{st}$, $\mathbf{R}_{sb}$, and $\mathbf{p}_{sb}$ between the two approaches have been plotted when the ballbot is operated freely under its drift vector field. Since the numerical integration error margin to be tolerated has been selected to be $10^{-7}$, these errors are well within the tolerance range.

#### 7.3.1.4 2D dynamics

We are interested in finding out how the equations of motion restrict to the plane spanned by the inertial $x$-$z$ axes of $\mathcal{W}$. In particular, we are going to

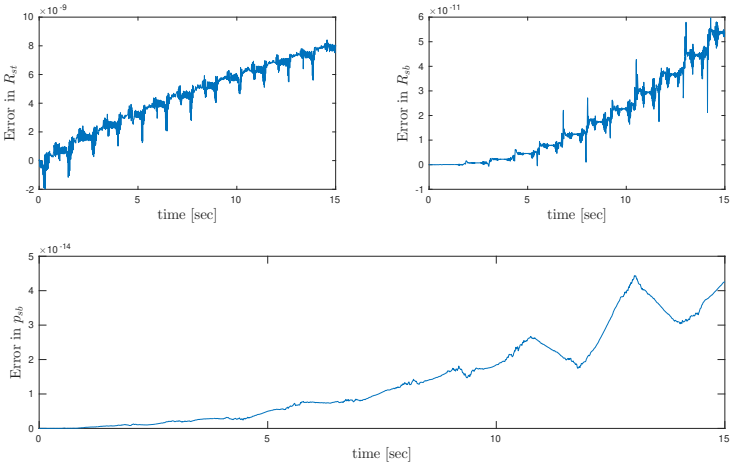


Fig. 7.9: Error between Euler-Poincaré equations and the conventional Lagrangian approach

use coordinates $x \in \mathbb{R}$ and $\theta \in \mathbb{R}$ on the circle for the rotation of the top with respect to $\mathcal{W}$ and the rotation of the top with respect to the ball, respectively. With this choice, the relevant quantities take on the values

$$\mathbf{R}_{st} = \mathbf{R}_{\mathbf{e}_2,x},\ \boldsymbol{\omega}_{st} = \dot{x}\mathbf{e}_2; \quad \mathbf{R}_{tb} = \mathbf{R}_{\mathbf{e}_2,\theta},\ \boldsymbol{\omega}_{sb} = \dot{\theta}\mathbf{e}_2,$$

where $R_{\mathbf{e}_2,\zeta}$ is the simple rotation matrix by $\zeta \in \mathbb{R}$ radians around the second standard basis vector $\mathbf{e}_2$. When restricted to the plane, the nonholonomic constraint becomes a holonomic one, and it is given by

$$\dot{\mathbf{p}}_{sb} = r_h \boldsymbol{\omega}_{sb} \times \mathbf{e}_3 = \begin{bmatrix} r_h \left(\dot{x} + \dot{\theta}\right) & 0 & 0 \end{bmatrix}^T. \tag{7.91}$$

Using these quantities, the Lagrangian (7.86) restricted to the inertial $x$-$z$ plane of $\mathcal{W}$ is computed to be

$$\begin{aligned} L = &\frac{1}{2}\left(I_t + m_t l^2 + m_t r_h l \cos(x) + I_b + (m_b + m_t) r_h^2\right) \dot{x}^2 \\ &+ \left(I_b + (m_b + m_t) r_h^2 + m_t r_h l \cos(x)\right) \dot{x}\dot{\theta} \\ &+ \frac{1}{2}\left(I_b + (m_b + m_t) r_h^2\right) \dot{\theta}^2 - m_t g l \cos x, \end{aligned}$$

where $I_b$ and $I_t$ are the components $(2,2)$ of the matrices $\mathbf{I}_b$ and $\mathbf{I}_t$, respectively. We can either use the conventional Euler-Lagrange equations with coordinates $(x, \theta)$ or directly the coordinate-invariant equations (7.90) derived in the previous section to compute the equations of motion of the ballbot

restricted to the plane. It is readily checked that these two distinct methods yield exactly the same equations, which are given by

$$\begin{aligned}\mathbf{M}(q)\ddot{\mathbf{q}}+\mathbf{C}(\mathbf{q},\dot{\mathbf{q}})\dot{\mathbf{q}}+\mathbf{g}(\mathbf{q}) &= \begin{bmatrix}\alpha+\gamma+2\beta\cos x & \alpha+\beta\cos x\\ \alpha+\beta\cos x & \alpha\end{bmatrix}\begin{bmatrix}\ddot{x}\\ \ddot{\theta}\end{bmatrix}\\ &\quad+\begin{bmatrix}-\beta\sin x\dot{x} & 0\\ -\beta\sin x\dot{x} & 0\end{bmatrix}\begin{bmatrix}\dot{x}\\ \dot{\theta}\end{bmatrix}+\begin{bmatrix}-\mu\sin x\\ 0\end{bmatrix}=\begin{bmatrix}0\\ 1\end{bmatrix}\tau,\end{aligned} \tag{7.92}$$

complemented by the rolling constraint (7.91) and with $\tau \in \mathbb{R}$ the control input. The various constants in these equations are given by $\alpha = I_b + (m_b + m_t)r_h^2$, $\beta = m_t r_h l$, $\gamma = I_t + m_t l^2$, and $\mu = m_t g l$. These equations correspond exactly to the ones given in [218].

### 7.3.2 Passivity based control design

When $\boldsymbol{\tau} = \mathbf{0_3}$, we can determine the equilibria of the ballbot using the equations of motion (7.90) with the rolling contraints (7.82) and (7.88). Along with the fact that the inertial $z$-axis rotation of the ball is assumed to be stationary, the rolling constraints yields $\dot{\mathbf{p}}_{sb} = \mathbf{0_3} \Longleftrightarrow \boldsymbol{\omega}_{\mathbf{sb}} = \boldsymbol{\omega}_{\mathbf{st}} + \bar{\boldsymbol{\omega}}_{\mathbf{tb}} = \mathbf{0_3}$. Inserting $\mathbf{p}_{sb} =$ constant and $\bar{\boldsymbol{\omega}}_{tb} = \mathbf{0_3}$ into the equations of motion (7.90) along with $\boldsymbol{\omega}_{st} = \mathbf{0_3}$ yields $\mathbf{e}_3 \times \boldsymbol{\gamma} = \mathbf{0_3}$. In other words, the uncontrolled equilibria of the ballbot are given by

$$\begin{aligned}E_{\pm} = \{&(\mathbf{p}_{sb}, \boldsymbol{\gamma}, \dot{\mathbf{p}}_{sb}, \boldsymbol{\omega}_{sb}, \boldsymbol{\omega}_{st}) \in TQ : \mathbf{p}_{sb} = \text{const},\ \boldsymbol{\gamma} = \pm\mathbf{e}_3\\ &\boldsymbol{\omega}_{st} = \bar{\boldsymbol{\omega}}_{tb} = \mathbf{0_3}, \dot{\mathbf{p}}_{\mathbf{sb}} = \mathbf{0_3}\}.\end{aligned}$$

Notice that $E_+$ corresponds to the upward equilibrium point, that is, the top points in the inertial positive $z$-direction and $E_-$ corresponds to the downward equilibrium point. The control objective is to asymptotically stabilize the set $E_+$.

#### 7.3.2.1 Passivity and energy considerations for the 2D ballbot

Partial feedback linearization of (7.92) is achieved by the following feedback

$$\begin{aligned}\tau = &\left(\alpha - \frac{(\alpha+\beta\cos(x))^2}{\alpha+\gamma+2\beta\cos(x)}\right)u + \left(\frac{\alpha+\beta\cos(x)}{\alpha+\gamma+2\beta\cos(x)} - 1\right)\beta\sin(x)\dot{x}^2\\ &+\frac{\mu(\alpha+\beta\cos(x))}{\alpha+\gamma+2\beta\cos(x)}\sin(x),\end{aligned}$$

which yields

$$(\alpha+\gamma+2\beta\cos(x))\,\ddot{x}-\beta\sin(x)\dot{x}^2-\mu\sin(x)= \\ -(\alpha+\beta\cos(x))\,u, \tag{7.93a}$$

$$\ddot{\theta}=u, \tag{7.93b}$$

with $u\in\mathbb{R}$ a virtual control input.

The following are two passive outputs

$$y_1=\dot{\theta}, \tag{7.94a}$$

$$y_2=-(\alpha+\beta\cos(x))\,\dot{x}, \tag{7.94b}$$

with the corresponding storage functions

$$H_1=\frac{1}{2}\dot{\theta}^2, \tag{7.95a}$$

$$H_2=\frac{1}{2}(\alpha+\gamma+2\beta\cos(x))\,\dot{x}^2+\mu\cos(x). \tag{7.95b}$$

#### 7.3.2.2 2D Energy-shaping control

Let us consider the following Lyapunov function candidate

$$H_d=k_e(k_1H_1+k_2H_2)+\frac{1}{2}k_k(k_1y_1+k_2y_2)^2+\frac{1}{2}k_I(k_1\theta-k_2(\alpha x+\beta\sin(x)))^2, \tag{7.96}$$

with $k_e,k_1,k_2,k_k,k_I>0$. Notice that this Lyapunov function candidate comes from the desired energy function that can be written as $H_d=\frac{1}{2}\begin{bmatrix}\dot{\theta} & \dot{x}\end{bmatrix}\mathbf{M}_d\begin{bmatrix}\dot{\theta}\\ \dot{x}\end{bmatrix}+V_d$, where

$$\mathbf{M}_d=\begin{bmatrix}k_ek_1+k_1^2k_k & -k_1k_2k_k\\ -k_1k_2k_k & k_ek_2(\alpha+\gamma+2\beta\cos(x))+k_2^2k_k(\alpha+\beta\cos(x))^2\end{bmatrix},$$

$$V_d=k_ek_2\mu\cos(x)+\frac{1}{2}k_I(k_1\theta-k_2(\alpha x+\beta\sin(x)))^2.$$

The conditions under which $\mathbf{M}_d$ and $V_d$ can be selected such that $H_d$ is a Lyapunov function are developed in the next subsection for the 3D-dynamics of the ballbot. Taking the Lie derivative of (7.96) along the solutions of (7.93),

we get

$$\dot{H}_d = (k_1 y_1 + k_2 y_2)\left[\left(k_e + k_1 k_k + k_2 k_k \frac{(\alpha + \beta\cos(x))^2}{\alpha + \gamma + 2\beta\cos(x)}\right) u + k_2 k_k \left(-(\alpha + \beta c_x)\left(\frac{\beta s_x}{\alpha + \gamma + 2\beta c_x}\dot{x}^2 + \frac{\mu s_x}{\alpha + \gamma + 2\beta c_x}\right) + \beta s_x \dot{x}^2\right) + k_I\left(k_1\theta - k_2\left(\alpha x + \beta s_x\right)\right)\right],$$

where $c_x$ and $s_x$ are shortened notations for $\cos(x)$ and $\sin(x)$, respectively.

Once we select the control as follows

$$u = -\frac{1}{k}\left[k_2 k_k \left(-(\alpha + \beta c_x)\left(\frac{\beta s_x}{\alpha + \gamma + 2\beta c_x}\dot{x}^2 + \frac{\mu s_x}{\alpha + \gamma + 2\beta c_x}\right) + \beta s_x \dot{x}^2\right) + k_I\left(k_1\theta - k_2\left(\alpha x + \beta s_x\right)\right) + k_p\left(k_1 y_1 + k_2 y_2\right)\right].$$

where $k = k_e + k_1 k_k + k_2 k_k \dfrac{(\alpha + \beta c_x)^2}{\alpha + \gamma + 2\beta c_x}$. The time derivative of $H_d$ becomes

$$\dot{H}_d \ = -k_p\left(k_1 y_1 + k_2 y_2\right)^2 \leq 0.$$

Once the detectability of the output $y = k_1 y_1 + k_2 y_2$ is proven, this implies that the desired equilibrium point is asymptotically stable. The detectability of this output is proven in the next section for the full dynamics of the ballbot. It is omitted in this section because that calculation can be applied to the 2D dynamics verbatim.

#### 7.3.2.3 Passivity and energy considerations for the 3D ballbot

Partial feedback linearization of the equations of motion (7.90) on the second factor yields

$$\begin{aligned}&\left(\mathbf{I}_t + m_t l^2\left(\mathbf{I}_3 - \boldsymbol{\gamma}\otimes\boldsymbol{\gamma}^T\right) + \mathbf{I}_b - (m_b + m_t) r_h^2 \hat{\mathbf{e}}_3^2 - m_t r_h l\left(\hat{\boldsymbol{\gamma}}\hat{\mathbf{e}}_3 + \hat{\mathbf{e}}_3\hat{\boldsymbol{\gamma}}\right)\right)\dot{\boldsymbol{\omega}}_{st} \\ &\quad + m_t l^2\left\langle\boldsymbol{\omega}_{st}, \boldsymbol{\gamma}\right\rangle\hat{\boldsymbol{\gamma}}\boldsymbol{\omega}_{st} + m_t r_h l \hat{\mathbf{e}}_3\hat{\boldsymbol{\omega}}_{st}^2\boldsymbol{\gamma} + \boldsymbol{\omega}_{st}\times\mathbf{I}_t\boldsymbol{\omega}_{st} - \boldsymbol{\omega}_{st} \\ &\quad \times\mathbf{I}_b\bar{\boldsymbol{\omega}}_{tb} - m_t g l\mathbf{e}_3\times\boldsymbol{\gamma} = -\left(\mathbf{I}_b - (m_b + m_t) r_h^2\hat{\mathbf{e}}_3^2 - m_t r_h l\hat{\boldsymbol{\gamma}}\hat{\mathbf{e}}_3\right)\mathbf{u},\end{aligned} \tag{7.97a}$$

$$\dot{\bar{\boldsymbol{\omega}}}_{tb} = \mathbf{u}, \tag{7.97b}$$

with $\mathbf{u} \in \mathbb{R}^3$ a virtual control input and where the feedback linearizing torque is given by

$$\begin{aligned}\boldsymbol{\tau} = \mathbf{R}_{st}^T \left(\mathbf{M}_{22} - \mathbf{M}_{12}^T \mathbf{M}_{11}^{-1} \mathbf{M}_{12}\right) \Big(\mathbf{u} + m_t r_h l \left(\mathbf{I}_3 - \mathbf{m}_{12}^T \mathbf{M}_{11}^{-1}\right) \hat{\mathbf{e}}_3 \hat{\boldsymbol{\omega}}_{st}^2 \boldsymbol{\gamma} \\ - \mathbf{M}_{12}^T \mathbf{M}_{11}^{-1} m_t l^2 \langle \boldsymbol{\omega}_{st}, \boldsymbol{\gamma} \rangle \hat{\boldsymbol{\gamma}} \boldsymbol{\omega}_{st} + \mathbf{M}_{12}^T \mathbf{M}_{11}^{-1} m_t g l \left(\mathbf{e}_3 \times \boldsymbol{\gamma}\right)\Big).\end{aligned}$$

The following are two passive outputs

$$\mathbf{y}_1 = \bar{\boldsymbol{\omega}}_{tb}, \tag{7.98a}$$

$$\mathbf{y}_2 = -\left(\mathbf{I}_b - (m_b + m_t) r_h^2 \hat{\mathbf{e}}_3^2 - \beta \hat{\mathbf{e}}_3 \hat{\boldsymbol{\gamma}}\right) \boldsymbol{\omega}_{st}. \tag{7.98b}$$

with the corresponding storage functions

$$H_1 = \frac{1}{2} \bar{\boldsymbol{\omega}}_{tb}^T \bar{\boldsymbol{\omega}}_{tb}, \tag{7.99a}$$

$$\begin{aligned}H_2 = \frac{1}{2} \boldsymbol{\omega}_{st}^T \left(\mathbf{I}_b - (m_b + m_t) r_h^2 \hat{\mathbf{e}}_3^2 - \beta \left(\hat{\boldsymbol{\gamma}} \hat{\mathbf{e}}_3 + \hat{\mathbf{e}}_3 \hat{\boldsymbol{\gamma}}\right) + \mathbf{I}_t + m_t l^2 \mathbf{I}_3\right) \boldsymbol{\omega}_{st} \\ - \frac{1}{2} m_t l^2 \left(\boldsymbol{\omega}_{st}^T \boldsymbol{\gamma}\right)^2 + \mu \mathbf{e}_3{}^T \boldsymbol{\gamma}.\end{aligned} \tag{7.99b}$$

The passivity of the pair $(bfy_1, H_1)$ is readily seen

$$\frac{\mathrm{d}H_1}{\mathrm{d}t} = \langle \bar{\boldsymbol{\omega}}_{tb}, \mathbf{u} \rangle = \langle \mathbf{y}_1, \mathbf{u} \rangle.$$

To prove the same statement for the pair $(y_2, H_2)$, we calculate

$$\begin{aligned}\frac{\mathrm{d}H_2}{\mathrm{d}t} &= \boldsymbol{\omega}_{st}^T \Big[\left(\mathbf{I}_b - (m_b + m_t) r_h^2 \hat{\mathbf{e}}_3^2 - \beta \left(\hat{\boldsymbol{\gamma}} \hat{\mathbf{e}}_3 + \hat{\mathbf{e}}_3 \hat{\boldsymbol{\gamma}}\right) + \mathbf{I}_t + m_t l^2\right) \dot{\boldsymbol{\omega}}_{st} - \mu \mathbf{e}_3 \\ &\qquad \times \boldsymbol{\gamma} + \frac{1}{2} \beta \left(\boldsymbol{\gamma} \times (\boldsymbol{\omega}_{st} \times (\mathbf{e}_3 \times \boldsymbol{\omega}_{st})) - \mathbf{e}_3 \times (\boldsymbol{\omega}_{st} \times (\boldsymbol{\gamma} \times \boldsymbol{\omega}_{st}))\right)\Big] \\ &= \boldsymbol{\omega}_{st}^T \Big[-\left(\mathbf{I}_b - (m_b + m_t) r_h^2 \hat{\mathbf{e}}_3^2 - \beta \hat{\boldsymbol{\gamma}} \hat{\mathbf{e}}_3\right) \mathbf{u} - \beta \left(\mathbf{e}_3 \times (\boldsymbol{\omega}_{st} \times (\boldsymbol{\omega}_{st} \times \boldsymbol{\gamma}))\right) \\ &\qquad - \frac{1}{2} \beta \left(2 \mathbf{e}_3 \times (\boldsymbol{\omega}_{st} \times (\boldsymbol{\gamma} \times \boldsymbol{\omega}_{st}))\right)\Big] \\ &= \left\langle -\left(\mathbf{I}_b - (m_b + m_t) r_h^2 \hat{\mathbf{e}}_3^2 - \beta \hat{\mathbf{e}}_3 \hat{\boldsymbol{\gamma}}\right) \boldsymbol{\omega}_{st}, \mathbf{u} \right\rangle = \langle \mathbf{y}_2, \mathbf{u} \rangle,\end{aligned}$$

where the second to the last step follows by noticing that the first two terms in the final expression below are orthogonal to $\boldsymbol{\omega}_{st}$

$$\begin{aligned}\boldsymbol{\gamma} \times (\boldsymbol{\omega}_{st} \times (\mathbf{e}_3 \times \boldsymbol{\omega}_{st})) &= -\boldsymbol{\omega}_{st} \times ((\mathbf{e}_3 \times \boldsymbol{\omega}_{st}) \times \boldsymbol{\gamma}) - (\mathbf{e}_3 \times \boldsymbol{\omega}_{st}) \times (\boldsymbol{\gamma} \times \boldsymbol{\omega}_{st}) \\ &= -\boldsymbol{\omega}_{st} \times ((\mathbf{e}_3 \times \boldsymbol{\omega}_{st}) \times \boldsymbol{\gamma}) - \boldsymbol{\omega}_{st} \\ &\quad \times ((\boldsymbol{\gamma} \times \boldsymbol{\omega}_{st}) \times \mathbf{e}_3) - \mathbf{e}_3 \times (\boldsymbol{\omega}_{st} \times (\boldsymbol{\gamma} \times \boldsymbol{\omega}_{st})).\end{aligned}$$

*Lemma 7.3.1* The integrals of the passive outputs can be computed to be

$$\dot{\bar{\boldsymbol{\theta}}}_{tb} = \mathbf{y}_1, \tag{7.100a}$$

$$\frac{\mathrm{d}}{\mathrm{d}t}\left\{-\mathbf{M}_{22}\boldsymbol{\theta}_{st} - \beta\mathbf{e}_3 \times \boldsymbol{\gamma}\right\} = \mathbf{y}_2, \tag{7.100b}$$

with $\bar{\boldsymbol{\theta}}_{tb}, \boldsymbol{\theta}_{st} \in \mathbb{R}^3$. □

*Proof* We first compute the integral of part of the second output, $-\beta\mathbf{e}_3 \times (\boldsymbol{\gamma} \times \boldsymbol{\omega}_{st})$. Let $\boldsymbol{\phi}(\boldsymbol{\gamma}, \boldsymbol{\omega}_{st}) = \beta\mathbf{e}_3 \times \boldsymbol{\gamma}$, then

$$\frac{\mathrm{d}\Phi}{\mathrm{d}t} = \beta\left(\mathbf{e}_3 \times \dot{\boldsymbol{\gamma}}\right) = -\beta\left(\mathbf{e}_3 \times (\boldsymbol{\gamma} \times \boldsymbol{\omega}_{st})\right). \tag{7.101}$$

To locally express the integral of the remaining terms, we use the exponential mapping from $\mathfrak{so}(3)$ to $SO(3)$ [183] to express the rotation so that

$$\mathbf{R}_{st} = \mathrm{e}^{\widehat{\boldsymbol{\theta}}_{st}}, \quad \mathbf{R}_{tb} = \mathrm{e}^{\widehat{\boldsymbol{\theta}}_{tb}} = \mathrm{e}^{-\widehat{\boldsymbol{\theta}}_{st}}\mathrm{e}^{\widehat{\boldsymbol{\theta}}_{sb}}.$$

Upon differentiation and utilization of the rigid body kinematics (7.83), we have

$$\begin{aligned}
\hat{\boldsymbol{\omega}}_{st} &= \dot{\mathbf{R}}_{st}\mathbf{R}_{st}^T = \dot{\hat{\boldsymbol{\theta}}}_{st}, \\
\hat{\bar{\boldsymbol{\omega}}}_{tb} &= \mathrm{Ad}_{\mathbf{R}_{st}}\hat{\boldsymbol{\omega}}_{tb} = \mathrm{Ad}_{\mathbf{R}_{st}}\left(\dot{\mathbf{R}}_{tb}\mathbf{R}_{tb}^T\right) = -\dot{\hat{\boldsymbol{\theta}}}_{st} + \dot{\hat{\boldsymbol{\theta}}}_{sb} =: \dot{\hat{\bar{\boldsymbol{\theta}}}}_{tb}.
\end{aligned}$$

Combining these with (7.101) yields the assertions of the lemma. □

#### 7.3.2.4 3D energy-shaping control

Let us consider the following Lyapunov function candidate

$$\begin{aligned}
H_d = k_e\left(k_1 H_1 + k_2 H_2\right) &+ \frac{1}{2}\|k_1\mathbf{y}_1 + k_2\mathbf{y}_2\|^2_{\mathbf{K}_k} \\
&+ \frac{1}{2}\|k_1\bar{\boldsymbol{\theta}}_{tb} + k_2\left(-\mathbf{M}_{22}\boldsymbol{\theta}_{st} - \beta\mathbf{e}_3 \times \boldsymbol{\gamma}\right)\|^2_{\mathbf{K}_I},
\end{aligned} \tag{7.102}$$

with $\mathbf{K}_k, \mathbf{K}_I \in \mathbb{R}^{3\times 3}$ constant matrices. Notice that this Lyapunov function candidate comes from a desired energy function that can be written as $H_d = \frac{1}{2}\begin{bmatrix}\boldsymbol{\omega}_{tb} & \boldsymbol{\omega}_{st}\end{bmatrix}\mathbf{M}_d\begin{bmatrix}\boldsymbol{\omega}_{tb} \\ \boldsymbol{\omega}_{st}\end{bmatrix} + V_d$, where

$$\mathbf{M}_d = \begin{bmatrix} k_e k_1\mathbf{I}_3 + k_1^2\mathbf{K}_k & -k_1 k_2\mathbf{K}_k\mathbf{M}_{12}^T \\ -k_1 k_2\mathbf{M}_{12}\mathbf{K}_k & k_e k_2\mathbf{M}_{11} + k_2^2\mathbf{K}_k\mathbf{M}_{12}\mathbf{M}_{12}^T \end{bmatrix}, \tag{7.103a}$$

$$V_d = k_e k_2 V + \frac{1}{2}\|k_1\bar{\boldsymbol{\theta}}_{tb} + k_2\left(-\mathbf{M}_{22}\boldsymbol{\theta}_{st} - \beta\mathbf{e}_3 \times \boldsymbol{\gamma}\right)\|^2_{\mathbf{K}_I}. \tag{7.103b}$$

Let $\mathbf{q}^* = (\mathbf{R}_{st}, \mathbf{R}_{tb}, \boldsymbol{\omega}_{st}, \bar{\boldsymbol{\omega}}_{tb}) = \left(\mathrm{e}^{\rho\hat{\mathbf{e}}_3}, \mathrm{e}^{\sigma\hat{\mathbf{e}}_3}, \mathbf{0_3}, \mathbf{0_3}\right)$, for some constants $\rho, \sigma \in \mathbb{R}$. In order to qualify $H_d$ as a Lyapunov function, we need to make

sure that $\mathbf{M}_d(\mathbf{q}^*)$ is posititve definite, $\delta V_d(\mathbf{q}^*) = 0$, $\delta^2 V_d(\mathbf{q}^*)$ is full rank along the directions orthogonal to the combined, but functionally related rotation of the ball and the top along the inertial vertical axis, and $\dot{H}_d \leq 0$. As long as the yaw rotation of the ball is restricted by its friction with the ground, by Lagrange-Dirichlet stability criterion, these conditions will ensure that both the ball and the top will converge to the desired orientation.

*Theorem 7.3.1* At $\mathbf{q}^*$, $V_d$ has a global minimum $V_d^*$, which is shared by a line of points characterized by a combined rotation of the ball and the top along the inertial vertical axis. □

*Proof* We observe from the expression of $V_d$ that it achieves a minimum only if each term individually achieves a minimum. While the minimum of the second term is zero, the minimum $k_e k_2 \mu$ of the first term $k_e k_2 \mu \mathbf{e}_3^T \boldsymbol{\gamma}$ is attained when $\boldsymbol{\gamma} = \mathbf{e}_3$, provided that $k_2 < 0$ and $k_e > 0$. Computing the first variation of $V_d$ yields

$$\begin{aligned}\delta V_d = {} & k_e k_2 \mu \boldsymbol{\eta}_{st}^T (\boldsymbol{\gamma} \times \mathbf{e}_3) \\ & + \left(k_1 \bar{\boldsymbol{\theta}}_{tb} - k_2 \left(\mathbf{M}_{22} \boldsymbol{\theta}_{st} + \beta \mathbf{e}_3 \times \boldsymbol{\gamma}\right)\right)^T \mathbf{K}_I \left(k_1 \bar{\boldsymbol{\eta}}_{tb} - k_2 \left(\mathbf{M}_{22} - \beta \hat{\mathbf{e}}_3 \hat{\boldsymbol{\gamma}}\right) \boldsymbol{\eta}_{st}\right),\end{aligned}$$

which vanishes at $\mathbf{q}^*$. Note that when $\boldsymbol{\theta}_{st} = \mathbf{0_3}$, it follows that $\boldsymbol{\gamma} = \mathbf{R}_{st}\mathbf{e}_3 = \mathrm{e}^{\hat{\boldsymbol{\theta}}_{st}}\mathbf{e}_3 = \mathrm{e}^{\hat{\mathbf{0_3}}}\mathbf{e}_3 = \mathbf{e}_3$.

Computing the second variation $\delta^2 V_d$ of $V_d$ at $\mathbf{q}^* = 0$ yields

$$\delta^2 V_d = k_e k_2 \boldsymbol{\eta}_{st}^T \hat{\mathbf{e}}_3^2 \boldsymbol{\eta}_{st} + \left\| k_1 \bar{\boldsymbol{\eta}}_{tb} - k_2 \left(\mathbf{M}_{22} - \beta \hat{\mathbf{e}}_3^2\right) \boldsymbol{\eta}_{st} \right\|_{\mathbf{K}_I}^2.$$

This expression shows that $\delta^2 V_d$ positive semidefinite and is degenerate only on the subspace spanned by $\boldsymbol{\eta}_{st} = \mathbf{e}_3$ and $\bar{\boldsymbol{\eta}}_{tb} = \dfrac{k_2}{k_1} \mathbf{M}_{22} \mathbf{e}_3$. Since $\mathbf{M}_{22}$ is a diagonal matrix, $\bar{\boldsymbol{\eta}}_{tb}$ is a multiple of $\mathbf{e}_3$ by a negative constant. □

The assumption that the yaw rotation of the ball is constrained by frictional forces implies that $\boldsymbol{\eta}_{sb}^T \mathbf{e}_3 = 0$. Since $\bar{\boldsymbol{\eta}}_{tb} = -\boldsymbol{\eta}_{st} + \boldsymbol{\eta}_{sb}$, it follows that $\bar{\boldsymbol{\eta}}_{tb}^T \mathbf{e}_3 = -\boldsymbol{\eta}_{st}^T \mathbf{e}_3$. Notice that this subspace and the nullspace of $\delta^2 V_d$ intersect only at the zero section of the tangent bundle (state space).

*Theorem 7.3.2* If the ballbot is *strongly inertially coupled* [297], *i.e.*, the rank of $\mathbf{M}_{12}(\mathbf{q})$ is three, then appropriate gains $k_e$, $k_1$, $k_2$, $\mathbf{K}_k$ can be chosen such that $\mathbf{M}_d(\mathbf{q})$ is positive definite. □

*Proof* $\mathbf{M}_d$ is positive definite if $k_e k_1 \mathbf{I}_3 + k_1^2 \mathbf{K}_k$ is positive definite and $\boldsymbol{\Delta}_{11}$ is positive definite, where $\boldsymbol{\Delta}_{11}$ is the Schur-complement of the $(1,1)$ block of $\mathbf{M}_d$, that is,

$$\boldsymbol{\Delta}_{11} = k_2 \left(k_e \mathbf{M}_{11} + k_2 \mathbf{M}_{12} \mathbf{K}_k \mathbf{M}_{12}^T\right) - k_1 k_2^2 \mathbf{M}_{12} \mathbf{K}_k \left(k_e \mathbf{I}_3 + k_1 \mathbf{K}_k\right)^{-1} \mathbf{K}_k \mathbf{M}_{12}^T.$$

The condition that $k_e k_1 \mathbf{I}_3 + k_1^2 \mathbf{K}_k$ is positive definite holds if $k_e, k_1 > 0$ and $\mathbf{K}_k$ is positive definite. These constraints on the gains will be in force in

the sequel. Let $\underline{\lambda}_k \in \mathbb{R}$ be the smallest eigenvalue of $\mathbf{K}_k$, $\bar{\lambda}_{11} \in \mathbb{R}$ denote the maximum of eigenvalue of $\mathbf{M}_{11}$, and $\underline{\lambda}_{12} \in \mathbb{R}$ denote the minimum eigenvalue of $\mathbf{M}_{12}\mathbf{M}_{12}^T$ as $\boldsymbol{\gamma}$ varies over $\mathbb{S}^2$. Note that when the hypothesis of the theorem holds, then $\underline{\lambda}_{12}$ is bounded away from zero. Since $k_2 < 0$ and $\mathbf{M}_{11}$ is positive definite, we have that $\boldsymbol{\Delta}_{11}$ is positive definite if and only if the matrix

$$k_e\mathbf{M}_{11} + k_2\mathbf{M}_{12}\mathbf{K}_k \left(\mathbf{I}_3 - k_1 \left(k_e\mathbf{I}_3 + k_1\mathbf{K}_k\right)^{-1} \mathbf{K}_k\right) \mathbf{M}_{12}^T$$

is negative definite. This implies that also the matrix

$$k_e\bar{\lambda}_{11}\mathbf{I}_3 + k_2\underline{\lambda}_k \left(1 - \frac{k_1\underline{\lambda}_k}{k_e + k_1\underline{\lambda}_k}\right) \mathbf{M}_{12}\mathbf{M}_{12}^T$$

is negative definite. Finally, this implies that

$$k_e\bar{\lambda}_{11} + k_2\underline{\lambda}_k \left(1 - \frac{k_1\underline{\lambda}_k}{k_e + k_1\underline{\lambda}_k}\right) \underline{\lambda}_{12} < 0.$$

This last implication shows that choosing the quantity $\dfrac{|k_2|\,\underline{\lambda}_k}{k_e}$ large enough ensures that the desired mass matrix $\mathbf{M}_d$ is positive definite at all points $\mathbf{q}$ where the system is strongly inertially coupled. □

Whether or not the system is strongly inertially coupled depends on the design of the mechanism. If the mass and inertia of the ball are large enough with respect to the top's mass, then this property holds everywhere in the configuration space. Therefore, the following control law achieves global asymptotic stability for those mechanism designs.

*Proposition 7.3.1* Consider the partially feedback linearized dynamics of the ballbot (7.97) in close loop with the control law

$$\mathbf{u} = -\mathbf{K}^{-1} \left[\mathbf{s} + \mathbf{K}_p \left(k_1\mathbf{y}_1 + k_2\mathbf{y}_2\right)\right], \tag{7.104}$$

with the expressions for the matrices $\mathbf{K} \in \mathbb{R}^{3\times3}$ and $\mathbf{s} \in \mathbb{R}^3$ that are as given in the proof, $\mathbf{K}_p \in \mathbb{R}^{3\times3}$ a positive definite matrix, and $k_1$, $k_2$ satisfy the conditions that render $\mathbf{M}_d$ a positive definite matrix, $\delta V_d(\mathbf{q}^*) = 0$, and $\delta^2 V_d(\mathbf{q}^*)$ a positive definite matrix.

Then, $\mathbf{q}^*$ is an asymptotically stable equilibrium of the closed-loop system. □

*Proof* Taking the Lie derivative of (7.102) along the solutions of (7.97) yields

$$\begin{aligned}\dot{H}_d = \Big\langle k_1\mathbf{y}_1 + k_2\mathbf{y}_2, \Big[\Big(k_e\mathbf{I}_3 + k_1\mathbf{K}_k + k_2\mathbf{K}_k\mathbf{M}_{12}^T\mathbf{M}_{11}^{-1}\mathbf{M}_{12}\Big)\,\mathbf{u} \\ + k_2\mathbf{K}_k\left(-\dot{\mathbf{M}}_{12}^T\boldsymbol{\omega}_{st} + \mathbf{M}_{12}^T\mathbf{M}_{11}^{-1}\left(\mathbf{c}_1 + \mathbf{g}_1\right)\right) \\ + \mathbf{K}_I\left(k_1\bar{\boldsymbol{\theta}}_{tb} + k_2\left(-\mathbf{M}_{22}\boldsymbol{\theta}_{st} - \beta\mathbf{e}_3\times\boldsymbol{\gamma}\right)\right)\Big]\Big\rangle \\ = \left\langle k_1\mathbf{y}_1 + k_2\mathbf{y}_2, \mathbf{K}\mathbf{u} + \mathbf{s}\right\rangle,\end{aligned}$$

where $\mathbf{c}_1 = m_t l^2\left\langle\boldsymbol{\omega}_{st},\boldsymbol{\gamma}\right\rangle\hat{\boldsymbol{\gamma}}\boldsymbol{\omega}_{st} + \beta\hat{\mathbf{e}}_3\hat{\boldsymbol{\omega}}_{st}^2\boldsymbol{\gamma} + \boldsymbol{\omega}_{st}\times\mathbf{I}_t\boldsymbol{\omega}_{st} - \boldsymbol{\omega}_{st}\times\mathbf{I}_b\hat{\boldsymbol{\omega}}_{tb}$, $\mathbf{g}_1 = -\mu\mathbf{e}_3\times\boldsymbol{\gamma}$. We thus select

$$\mathbf{u} = -\mathbf{K}^{-1}\left[\mathbf{s} + \mathbf{K}_p\left(k_1\mathbf{y}_1 + k_2\mathbf{y}_2\right)\right], \tag{7.105}$$

where $\mathbf{K} = \Big(k_e\mathbf{I}_3 + k_1\mathbf{K}_k + k_2\mathbf{K}_k\mathbf{M}_{12}^T\mathbf{M}_{11}^{-1}\mathbf{M}_{12}\Big)$, $\mathbf{s}$ consists of all the terms not multiplied by $\mathbf{u}$ in the second factor of the natural pairing and $\mathbf{K}_p$ being positive definite, yielding

$$\dot{H}_d = -\|k_1\mathbf{y}_1 + k_2\mathbf{y}_2\|_{\mathbf{K}_p}^2.$$

This implies that $k_1\mathbf{y}_1 + k_2\mathbf{y}_2 \xrightarrow[t\to\infty]{} \mathbf{0_3}$. Let us analyze the smallest invariant set within $\mathcal{E} = \{k_1\mathbf{y}_1 + k_2\mathbf{y}_2 = \mathbf{0_3}\}$. We have

$$\mathbf{0_3} = \mathbf{k_1K_k\dot{y}_1} + \mathbf{k_2K_k\dot{y}_2} = \Big(\mathbf{k_1K_k} + \mathbf{k_2K_kM_{12}^TM_{11}^{-1}M_{12}}\Big)\,\mathbf{u} + \boldsymbol{\delta_1},$$

where $\boldsymbol{\delta}_1 = k_2\mathbf{K}_k\Big(-\dot{\mathbf{M}}_{12}^T\boldsymbol{\omega}_{st} + \mathbf{M}_{12}^T\mathbf{m}_{11}^{-1}\left(\mathbf{c}_1 + \mathbf{g}_1\right)\Big)$. Thus, we can write the above equation as $\left(\mathbf{K} - k_e\mathbf{I}_3\right)\mathbf{u} = -\boldsymbol{\delta}_1$. From the control law (7.104), we have $\mathbf{K}\mathbf{u} = -\left(\boldsymbol{\delta}_1 + \boldsymbol{\delta}_2\right)$, where $\boldsymbol{\delta}_2 = \mathbf{K}_I\left(k_1\bar{\boldsymbol{\theta}}_{tb} + k_2\left(-\mathbf{M}_{22}\boldsymbol{\theta}_{st} - \beta\mathbf{e}_3\times\boldsymbol{\gamma}\right)\right)$. Therefore, from the following two equations

$$\begin{aligned}\left(\mathbf{K} - k_e\mathbf{I}_3\right)\mathbf{u} &= -\boldsymbol{\delta}_1, \\ \mathbf{K}\mathbf{u} &= -\left(\boldsymbol{\delta}_1 + \boldsymbol{\delta}_2\right),\end{aligned}$$

we deduce that $\mathbf{u} = -\dfrac{1}{k_e}\boldsymbol{\delta}_2$ on $\mathcal{E}$. Plugging this into (7.97), shows that the first of these equations is unstable unless $\mathbf{u} = \boldsymbol{\delta}_2 = \mathbf{0_3}$. This implies $\bar{\boldsymbol{\omega}}_{tb} = \text{constant} = \mathbf{0_3}$, which, in turn, implies $\boldsymbol{\omega}_{st} = \mathbf{0_3}$ because otherwise its dynamics would again be unstable. This discussion shows that the system asymptotically converges to an equilibrium point. Since the closed-loop system comes from a Lagrangian system, it is readily shown that, the only stable equilibrium point is the upward equilibrium point, with $\boldsymbol{\theta}_{st} = \begin{bmatrix}0 & 0 & \text{constant}\end{bmatrix}^T$ and $\boldsymbol{\theta}_{tb} = \begin{bmatrix}0 & 0 & \text{constant}\end{bmatrix}^T$, where the inertial $z$-axis rotation of the system goes to a certain constant because this motion is uncontrollable. □

#### 7.3.2.5 Controlling the ball position

We can use a similar technique as in Section 7.3.2.4 to control the position of the ball as well as the upward equilibrium point of the top. In order to do this, we start from (7.97) and switch to the error system dynamics, with the error defined by $\bar{\mathbf{e}}_{tb} = \bar{\boldsymbol{\omega}}_{tb} - \bar{\boldsymbol{\omega}}^d_{tb}$, where $\bar{\boldsymbol{\omega}}^d_{tb}$ is the desired angular velocity of the ball with respect to the top expressed in $\mathcal{W}$. We compute this quantity from the desired angular velocity of the ball with respect to the spatial frame, $\boldsymbol{\omega}^d_{sb} \in \mathbb{R}^3$, which is, in turn, computed from the rolling constraint (7.82). In order to get $\mathbf{p}_{sb} \to \mathbf{p}^d_{sb}$, where $\mathbf{p}^d_{sb} \in \mathbb{R}^3$ is the desired position of the ball on the $x$-$y$ plane (the $z$ component is a constant), we would like the rolling constraint equation (7.82) to look like

$$\dot{\mathbf{p}}_{sb} = r_h \boldsymbol{\omega}^d_{sb} \times \mathbf{e}_3 = k_t \hat{\mathbf{e}}_3^2 \left(\mathbf{p}_{sb} - \mathbf{p}^d_{sb}\right).$$

As a result, we set $\boldsymbol{\omega}^d_{sb} = -\dfrac{k_t}{r_h} \hat{\mathbf{e}}_3 \left(\mathbf{p}_{sb} - \mathbf{p}^d_{sb}\right)$, where $k_t > 0$. This implies that the desired angular velocity of the ball with respect to the top expressed in $\mathcal{W}$ is, $\bar{\boldsymbol{\omega}}^d_{tb} = \boldsymbol{\omega}^d_{sb} - \boldsymbol{\omega}_{st}$. We use (7.82) in the time derivative of this relation to get

$$\dot{\bar{\boldsymbol{\omega}}}^d_{tb} = \dot{\boldsymbol{\omega}}^d_{sb} - \dot{\boldsymbol{\omega}}_{st} = k_t \hat{\mathbf{e}}_3^2 \left(\bar{\boldsymbol{\omega}}_{tb} + \boldsymbol{\omega}_{st}\right) - \dot{\boldsymbol{\omega}}_{st}. \tag{7.106}$$

We set the the control $\mathbf{u}$ in equation (7.97) to $\mathbf{u} = \dot{\bar{\boldsymbol{\omega}}}^d_{tb} + \mathbf{v}$, with $\mathbf{v} \in \mathbb{R}^3$ a virtual input, which yields the error system dynamics

$$\left(\mathbf{M}_{11} - \mathbf{M}_{12}\right) \dot{\boldsymbol{\omega}}_{st} + \mathbf{c}_2 + \mathbf{g}_1 = -\mathbf{M}_{12}\mathbf{v}, \tag{7.107a}$$

$$\dot{\bar{\mathbf{e}}}_{tb} = \mathbf{v}, \tag{7.107b}$$

where $\mathbf{c}_2 = \mathbf{c}_1 + k_t \mathbf{M}_{12} \hat{\mathbf{e}}_3^2 \left(\bar{\boldsymbol{\omega}}_{tb} + \boldsymbol{\omega}_{st}\right)$. Solving (7.107) for $\dot{\boldsymbol{\omega}}_{st}$ and substituting into (7.106), we derive the form of the control $\mathbf{u}$ as

$$\begin{aligned}\mathbf{u} = &\left(\mathbf{I}_3 + \left(\mathbf{M}_{11} - \mathbf{M}_{12}\right)^{-1} \mathbf{M}_{12}\right) \mathbf{v} \\ &+ \left(\mathbf{M}_{11} - \mathbf{M}_{12}\right)^{-1} \left(\mathbf{c}_2 + \mathbf{g}_1\right) + k_t \hat{\mathbf{e}}_3^2 \left(\bar{\boldsymbol{\omega}}_{tb} + \boldsymbol{\omega}_{st}\right).\end{aligned}$$

We identify a passive output $\mathbf{y}_1 = \bar{\mathbf{e}}_{tb}$ with the storage function $H_1 = \dfrac{1}{2} \bar{\mathbf{e}}_{tb}^T \bar{\mathbf{e}}_{tb}$. We keep the second output $\mathbf{y}_2 = -\mathbf{M}_{12}^T \boldsymbol{\omega}_{st}$ and modify its storage to $H_2' = H_2 - \boldsymbol{\omega}_{st}^T \mathbf{M}_{12} \boldsymbol{\omega}_{st}$. Note that this output with the storage function $H_2'$ is not passive any more due to the additional terms appearing in $\mathbf{c}_2$. It is also important to note that, we do not need to asymptotically stabilize the orientation of the ball to a desired value. We would rather asymptotically stabilize $\bar{\mathbf{e}}_{tb}$ to zero, which implies $\boldsymbol{\omega}_{sb} \to \boldsymbol{\omega}^d_{sb}$, which, in turn, asymptotically stabilizes $\mathbf{p}_{sb}$ to $\mathbf{p}^d_{sb}$. This observation implies that, we only need to devise a desired potential energy which has $\boldsymbol{\gamma} = \mathbf{e}_3$ a point of minimum. This is easily achieved by setting $V_d = k_e k_2 V$. Recall that the product $k_e k_2$ is negative and

since the original potential energy $V$ has a minimum at $\boldsymbol{\gamma} = -\mathbf{e}_3$, this desired potential energy is good enough.

To shape the kinetic energy of the system, we use the same desired mass matrix as the one (7.103) used in the previous subsection. We use the following desired Hamiltonian (energy) for the closed loop system

$$H_d = k_e \left(k_1 H_1 + k_2 H_2'\right) + \frac{1}{2}\|k_1\mathbf{y}_1 + k_2\mathbf{y}_2\|^2_{\mathbf{K}_k} + \frac{1}{2}\left\langle \mathbf{p}_{sb} - \mathbf{p}^d_{sb}, \mathbf{p}_{sb} - \mathbf{p}^d_{sb}\right\rangle.$$

Proceeding analogously to Proposition 7.3.1, we compute the time derivative of $H_d$ to be

$$\begin{aligned}\dot{H}_d = \Big\langle k_1\mathbf{y}_1 + k_2\mathbf{y}_2, \Big[\Big(k_e\mathbf{I}_3 + k_1\mathbf{K}_k + k_2\mathbf{K}_k\mathbf{M}_{12}^T\left(\mathbf{M}_{11} - \mathbf{M}_{12}\right)^{-1}\mathbf{M}_{12}\Big)\mathbf{v} \\ + k_2\mathbf{K}_k\left(-\dot{\mathbf{M}}_{12}^T\boldsymbol{\omega}_{st} + \mathbf{M}_{12}^T\left(\mathbf{M}_{11} - \mathbf{M}_{12}\right)^{-1}\left(\mathbf{c}_2 + \mathbf{g}_1\right)\right)\Big]\Big\rangle \\ - \frac{\beta}{2}\left\langle \boldsymbol{\omega}_{st}, \hat{\mathbf{e}}_3^2\hat{\boldsymbol{\omega}}_{st}^2\boldsymbol{\gamma}\right\rangle + \left\langle -k_e k_t\hat{\mathbf{e}}_3^2\left(\mathbf{y}_1 - \frac{k_t}{r_h}\hat{\mathbf{e}}_3\left(\mathbf{p}_{sb} - \mathbf{p}^d_{sb}\right)\right), k_2\mathbf{y}_2\right\rangle \\ + \left\langle k_t\hat{\mathbf{e}}_3^2\left(\mathbf{p}_{sb} - \mathbf{p}^d_{sb}\right), \mathbf{p}_{sb} - \mathbf{p}^d_{sb}\right\rangle + \left\langle r_h\mathbf{y}_1, \hat{\mathbf{e}}_3\left(\mathbf{p}_{sb} - \mathbf{p}^d_{sb}\right)\right\rangle,\end{aligned}$$

where the second and third natural pairings arise because of the extra terms in the new Coriolis term, $\mathbf{c}_2$. We select the virtual input term $\mathbf{v}$ as

$$\mathbf{v} = -\mathbf{K}_b^{-1}\left[\mathbf{s}_b + \mathbf{K}_p\left(k_1\mathbf{y}_1 + k_2\mathbf{y}_2\right) + \frac{k_e k_t^2}{r_h}\hat{\mathbf{e}}_3^2\left(\mathbf{p}_{sb} - \mathbf{p}^d_{sb}\right)\right], \quad (7.108)$$

where $\mathbf{K}_b = \Big(k_e\mathbf{I}_3 + k_1\mathbf{K}_k + k_2\mathbf{K}_k\mathbf{M}_{12}^T\left(\mathbf{M}_{11} - \mathbf{M}_{12}\right)^{-1}\mathbf{M}_{12}\Big)$, $\mathbf{s}_b \in \mathbb{R}^3$ consists of all the terms not multiplied by $\mathbf{v}$ in the second factor of the first natural pairing, and $\mathbf{K}_p \in \mathbb{R}^{3\times 3}$ is a positive definite constant matrix. This selection yields to the following expression for the time derivative of $H_d$ along the solutions of the system

$$\begin{aligned}\dot{H}_d = -\|k_1\mathbf{y}_1 + k_2\mathbf{y}_2\|^2_{\mathbf{K}_p} + k_e k_2 k_t\left\langle \hat{\mathbf{e}}_3^2\mathbf{y}_1, \mathbf{y}_2\right\rangle - \frac{\beta}{2}\left\langle \boldsymbol{\omega}_{st}, \hat{\mathbf{e}}_3^2\hat{\boldsymbol{\omega}}_{st}^2\boldsymbol{\gamma}\right\rangle \\ + k_t\left\langle \hat{\mathbf{e}}_3^2\left(\mathbf{p}_{sb} - \mathbf{p}^d_{sb}\right), \mathbf{p}_{sb} - \mathbf{p}^d_{sb}\right\rangle + \left\langle \left(r_h - \frac{k_1 k_e k_t^2}{r_h}\right)\mathbf{y}_1, \hat{\mathbf{e}}_3\left(\mathbf{p}_{sb} - \mathbf{p}^d_{sb}\right)\right\rangle.\end{aligned}$$

Selecting $k_t = \dfrac{r_h}{\sqrt{k_1 k_e}}$ ensures that the last natural pairing in this expression vanishes. While the first natural pairing may be absorbed into the very first term, using the Cauchy-Schwarz inequality, by a proper selection of the gain $\mathbf{K}_p$, the second natural pairing satisfies the linear growth condition as long as strong inertial coupling condition is satisfied. As a result, this pairing may also be dominated by the first term semi-globally by increasing the magnitude of the gain $k_2$. These arguments prove that $\dot{H}_d \leq 0$. Since the detectability of the output $\mathbf{y} = k_1\mathbf{y}_1 + k_2\mathbf{y}_2$ is proven in exactly the same way as in the proof of Proposition 7.3.1, we can summarize the result in the following proposition

Table 7.3: System parameters

| Parameter | Symbol | Value |
|---|---|---|
| Ball radius | $r_h$ | 0.1058 m |
| Ball mass | $m_b$ | 244 kg |
| Ball inertia | $I_b$ | 1.821 kg·m$^2$ |
| Top center of mass height | $l$ | 0.69 m |
| Roll moment of inertia | $I_{t,11}$ | 12.59 kg·m$^2$ |
| Pitch moment of inertia | $I_{t,22}$ | 12.48 kg·m$^2$ |
| Yaw moment of inertia | $I_{t,33}$ | 0.66 kg·m$^2$ |
| Top mass | $m_t$ | 51.66 kg |

*Proposition 7.3.2* Consider the partially feedback linearized dynamics of the ballbot (7.97) in closed loop with the control law

$$\mathbf{v} = -\mathbf{K}_b^{-1}\left[\mathbf{s}_b + \mathbf{K}_p\left(k_1\mathbf{y}_1 + k_2\mathbf{y}_2\right) + \frac{k_e k_t^2}{r_h}\hat{e}_3^2\left(\mathbf{p}_{sb} - \mathbf{p}_{sb}^d\right)\right], \tag{7.109a}$$

$$\begin{aligned}\mathbf{u} = &\left(\mathbf{I}_3 + \left(\mathbf{M}_{11} - \mathbf{M}_{12}\right)^{-1}\mathbf{M}_{12}\right)\mathbf{v} \\ &+ \left(\mathbf{M}_{11} - \mathbf{M}_{12}\right)^{-1}\left(\mathbf{c}_2 + \mathbf{g}_1\right) + k_t\hat{\mathbf{e}}_3^2\left(\bar{\boldsymbol{\omega}}_{tb} + \boldsymbol{\omega}_{st}\right),\end{aligned} \tag{7.109b}$$

with the expressions for $\mathbf{K}_b$, $\mathbf{s}_b$ and $k_t$ are as given above the proposition, $\mathbf{K}_p$ a positive definite matrix, and $k_1$, $k_2$ satisfy the conditions that render $\mathbf{M}_d$ positive definite, $\delta V_d(\boldsymbol{\gamma} = \mathbf{e}_3) = 0$, and $\delta^2 V_d(\boldsymbol{\gamma} = \mathbf{e}_3)$ a positive definite matrix.

Then, $\boldsymbol{\gamma} = \mathbf{e}_3$, $\boldsymbol{\omega}_{st} = \mathbf{0_3}$, $\bar{\boldsymbol{\omega}}_{tb} = \mathbf{0_3}$, and $\mathbf{p}_{sb} = \mathbf{p}_{sb}^d$ is an asymptotically stable equilibrium of the closed-loop system. □

*Remark 7.1* Although the control design in the section is inspired by the development in [81], the technique presented in that work cannot be applied verbatim. The fundamental reason for this shortcoming is that the dynamics (7.90) is not derived directly from Euler-Lagrange equations, but are reduced to yield the Euler-Poincaré equations. Consequently, the construction of a second passive output in (7.98), a corresponding storage function in (7.99) and an integral of this passive output (7.100) has to be novelly performed. Once these quantities have been obtained, we can construct the Lyapunov function (7.102).

### 7.3.3 Numerical examples

The inertial properties of the ballbot that are utilized in the simulations are given in Table 7.3.

First, simulation results for the ballbot whose dynamics is restricted to the 2D $x$-$z$ plane are presented. The initial conditions and the control gains used

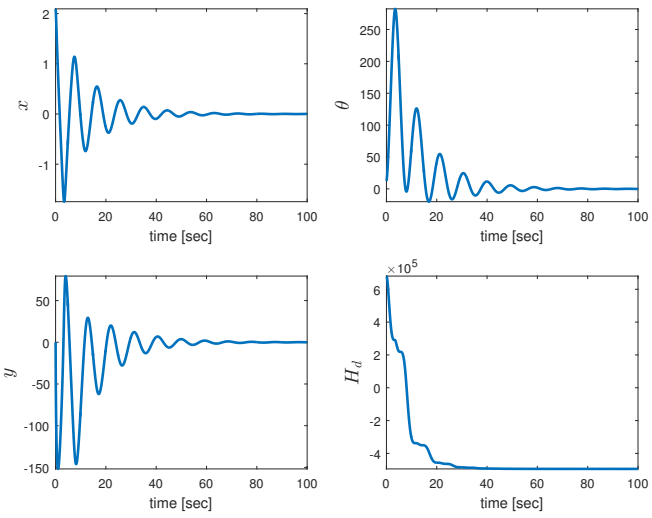


Fig. 7.10: Asymptotic stabilization of the 2D Ballbot

in the simulation are given in the first row of Table 7.4. The corresponding simulation results are shown in Fig. 7.10. The top two plots illustrate the convergence of the orientation of the top and the ball, in other words, the fact that $x$ and $\theta$ tend both to zero. The bottom left plot shows the evolution of the passive output $y = k_1 y_1 + k_2 y_2$, while the bottom right plot shows the evolution of the closed-loop energy functional $H_d$ (7.96).

Second, simulation results are presented that show the response of the ballbot to a feedback control (7.104). In this simulation, the initial conditions and the control gains are given by the second row of Table 7.4. Notice that the initial conditions are quite far away from the desired upward equilibrium $\mathbf{R}_{st} = \mathrm{e}^{\rho \hat{\mathbf{e}}_3}$ and the desired ball orientation $\mathbf{R}_{sb} = \mathrm{e}^{\sigma \hat{\mathbf{e}}_3}$, where $\rho$ and $\sigma$ are constant real numbers. On the left of Fig. 7.11, we illustrate the asymptotic stabilization. The top two plots illustrates the fact that both the ball and the top move to an orientation such that $\mathbf{R}_{st} e_3 = \mathbf{e}_3$ and $\mathbf{R}_{sb} e_3 = \mathbf{e}_3$, which is another way to state that $\mathbf{R}_{st} = \mathrm{e}^{\rho \hat{\mathbf{e}}_3}$ and $\mathbf{R}_{sb} = \mathrm{e}^{\sigma \hat{\mathbf{e}}_3}$ for some constant numbers $\rho$ and $\sigma$. The bottom left plot shows the evolution of the passive output $\mathbf{y} = k_1 \mathbf{y}_1 + k_2 \mathbf{y}_2$, while the bottom right plot shows the evolution of the closed loop energy functional $H_d$ (7.102). The path tracked by the ballbot on the plane is shown on the right in Fig. 7.11.

Finally, we present the simulation results that use the controller (7.109), designed to stabilize the position of the ball along with the upward equilibrium of the top. The initial conditions and the control gains are selected as the third row of Table 7.4. On the left of Fig. 7.12, the top left plot shows

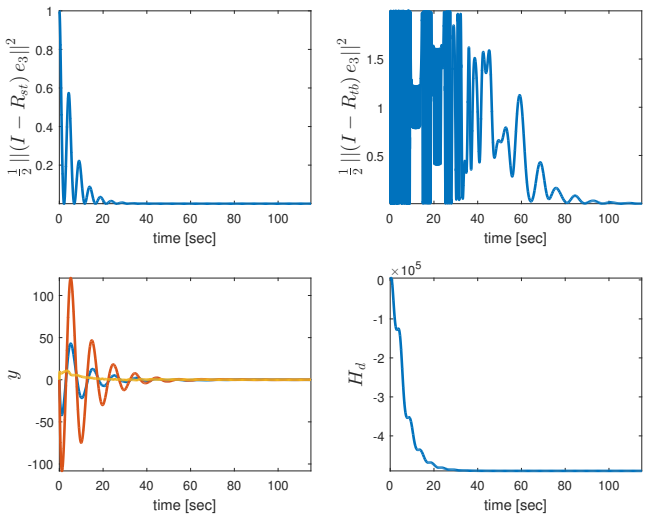


(a)

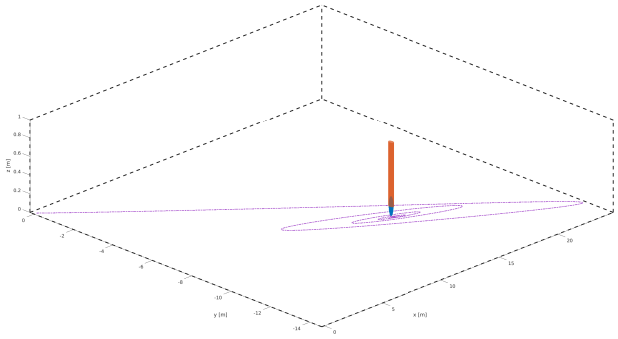

(b)

Fig. 7.11: (a) Time evolution of quantities of interest (b) The path tracked by the Ballbot

that the top asymptotically converges to the upward equilibrium point, where $\boldsymbol{\gamma} = \mathbf{e}_3$. The top left figure depicts the evolution of the position error of the ball, which converges to zero, indicating that $\mathbf{p}_{sb} \to \mathbf{p}^d_{sb}$. Additionally, while the bottom left plot shows that the passive output is asymptotically driven to zero, the bottom right plot shows that the closed-loop energy function $H_d$ converges to its minimum value, as expected due to the detectability of the passive output $\mathbf{y}$. Again, the path tracked by the ballbot on the plane is shown on the right of Fig. 7.12.

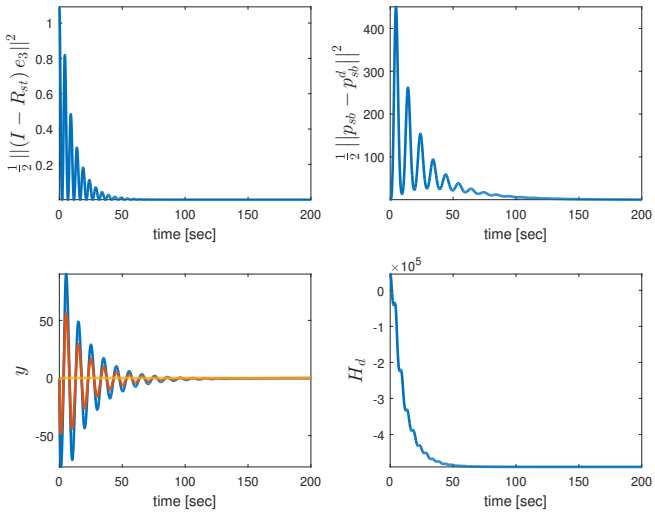


(a)

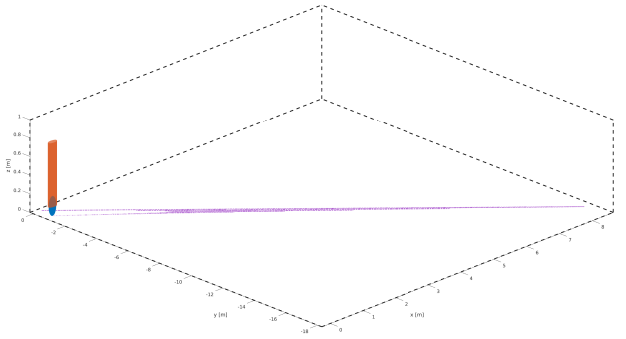

(b)

Fig. 7.12: (a) Time evolution of quantities of interest. (b) The path tracked by the Ballbot

## 7.4 Discussion and conclusion

This chapter investigated the control design for nonprehensile rolling manipulation dealing with nonholonomic constraints. Two systems were addressed, namely, the hula-hoop and the ballbot.

The considered robotic hula-hoop is an underactuated mechanical system subject to second-order nonholonomic constraints. We designed a locally sta-

ble controller scheme by exploiting the null space of the inertia coupling matrices, making it possible to simultaneously satisfy the control objective of (*i*) spinning the hoop at a desired angular velocity on the desired position over the pole surface and (*ii*) stabilizing the pole coordinates. A formal proof that guarantees locally ultimate boundedness of the hoop coordinates was presented, with arbitrary small ultimate bound on the tracking error and boundedness of the pole coordinates. To validate the proposed approach, we presented a numerical simulation that showed our solution's good performance. The main challenges for the experimental setup are the necessity of a high-speed reconstruction of the hoop position and orientation (in the simulation is was considered to be implemented at a 20 Hz rate) with good resolution and the high velocities and acceleration required for the actuator (*e.g.*, for the humanoid-like robot used in the simulations).

The ballbot robotic system is made of an actuated ball with a top. A reduced set of dynamic equations, whose configuration space is $Q = \mathbb{R}^2 \times SO(3) \times SO(3)$, was derived. These 10 first-order ODEs can express the system's motion comprehensibly, given the kinematic relations that the system has to satisfy. We can analyze dynamic properties and derive control laws that achieve asymptotic stabilization for several purposes thanks to the compact form of these equations of motion. In particular, we identified two passive outputs for the restricted 2D dynamics and the full 3D dynamics, which were then used to devise energy-shaping control laws making the system behave as a new Lagrangian system whose desired equilibrium point is asymptotically stable. The basin of attraction was shown to be global as long as the mechanism is designed to be strongly inertially coupled. We emphasize that modeling, analysis, and computations can be carried out directly in a geometric coordinate-free framework, as illustrated for the ballbot in this chapter. This fact facilitates the analysis of the dynamics and control synthesis for complex systems such as the ballbot.

| | Initial conditions | | Control gains | | |
|---|---|---|---|---|---|
| Sim 1 | $x(0) = \frac{2\pi}{3}$ | $\theta(0) = 4\pi$ | $k_1 = 5$ | $k_2 = -70$ | $k_e = 20$ |
| | $\dot{x}(0) = 0$ | $\dot{\theta} = 0$ | $k_k = 11$ | $k_p = 10$ | $k_I = 1$ |
| Sim 2 | $\mathbf{R}_{st}(0) = \mathbf{R}_{y,\frac{\pi}{3}}\mathbf{R}_{x,-\frac{\pi}{2}}$ | $\mathbf{R}_{sb}(0) = \mathbf{I}_3$ | $k_1 = 5$ | $k_2 = -70$ | $k_e = 20$ |
| | $\boldsymbol{\omega}_{st}(0) = \boldsymbol{\omega}_{sb} = \mathbf{0_3}$ | $\mathbf{p}_{sb} = \mathbf{0_3}$ | $\mathbf{K}_k = 11\mathbf{I}_3$ | $= \mathbf{K}_p = 10\mathbf{I}_3$ | $\mathbf{K}_I = \mathbf{I}_3$ |
| Sim 3 | $\mathbf{R}_{st}(0) = \mathbf{R}_{z,\frac{4\pi}{3}}\mathbf{R}_{y,1.74}\mathbf{R}_{x,1}$ | $= \mathbf{R}_{sb}(0) = \mathbf{I}_3$ | $k_1 = 5$ | $k_2 = -70$ | $k_e = 20$ |
| | $\boldsymbol{\omega}_{st}(0) = \boldsymbol{\omega}_{sb} = \mathbf{0_3}$ | $\tilde{\mathbf{p}}_{sb}(0) = (\frac{1}{4}, \frac{2}{y}, 0)$ | $\mathbf{K}_k = 11\mathbf{I}_3$ | $= \mathbf{K}_p = 7.5\mathbf{I}_3$ | $k_t \frac{r}{\sqrt{k_1 k_e}} =$ |

Table 7.4: Initial conditions and control gains